VALIDATION AND PARAMETRIC STUDIES OF DISCRETE VORTEX
METHOD ON FLOW AROUND BLUFF BODIES

A THESIS SUBMITTED TO
THE GRADUATE SCHOOL OF NATURAL AND APPLIED SCIENCES
OF
MIDDLE EAST TECHNICAL UNIVERSITY

BY

RUHİ DENİZ YALÇIN

IN PARTIAL FULFILLMENT OF THE REQUIREMENTS
FOR
THE DEGREE OF MASTER OF SCIENCE
IN
CIVIL ENGINEERING

JULY 2019

Approval of the thesis:

VALIDATION AND PARAMETRIC STUDIES OF DISCRETE VORTEX METHOD ON FLOW AROUND BLUFF BODIES

submitted by **RUHİ DENİZ YALÇIN** in partial fulfillment of the requirements for the degree of **Master of Science in Civil Engineering Department, Middle East Technical University** by,

Prof. Dr. Halil Kalıpçılar
Dean, Graduate School of **Natural and Applied Sciences**   _____

Prof. Dr. Ahmet Türer
Head of Department, **Civil Engineering**   _____

Prof. Dr. Özgür Kurç
Supervisor, **Civil Engineering, METU**   _____

Examining Committee Members:

Prof. Dr. Kağan Tuncay
Civil Engineering, METU   _____

Prof. Dr. Özgür Kurç
Civil Engineering, METU   _____

Prof. Dr. Afşin Sarıtaş
Civil Engineering, METU   _____

Assoc. Prof. Dr. Hakan Ahmet Argeşo
Manufacturing Engineering, ATILIM   _____

Assoc. Prof. Dr. Nilay Sezer Uzol
Department of Aerospace Engineering, METU   _____

Date: 03.07.2019

I hereby declare that all information in this document has been obtained and presented in accordance with academic rules and ethical conduct. I also declare that, as required by these rules and conduct, I have fully cited and referenced all material and results that are not original to this work.

Name, Surname: Ruhi Deniz Yalçın

Signature:

ABSTRACT

VALIDATION AND PARAMETRIC STUDIES OF DISCRETE VORTEX METHOD ON FLOW AROUND BLUFF BODIES

Yalçın, Ruhi Deniz
Master of Science, Civil Engineering
Supervisor: Prof. Dr. Özgür Kurç

July 2019, 87 pages

Aerodynamical analysis of rectangular sections, and a bridge deck section are investigated by 2D Discrete Vortex Method for two dimensional, unsteady, incompressible and viscous flows which is developed using C++ programming language. The numerical algorithm and methodology are explained in detail. The numerical method is validated by comparing its results with several experimental results. Moreover, the sensitivity of numerical solutions is examined by some control parameters which inhibit the most significant effect on the numerical solutions.

Keywords: Computational Fluid Dynamics, Bluff Body Aerodynamics, Discrete Vortex Method

ÖZ

AYRIK GİRDAP YÖNTEMİNİN KÜT CİSİMLER ETRAFINDAKİ AKIŞ ÜZERİNDE DOĞRULAMASI VE PARAMETRİK ÇALIŞMALARI

Yalçın, Ruhi Deniz
Yüksek Lisans, İnşaat Mühendisliği
Tez Danışmanı: Prof. Dr. Özgür Kurç

Temmuz 2019, 87 sayfa

Diktörtgen ve köprü tabliye kesitlerinin aerodinamik analizleri, iki boyutlu, zamana bağlı, sıkıştırılamayan ve viskoz akışlar için C++ programlama dili ile geliştirilmiş olan Ayrık Girdap Yöntemi ile incelenmiştir. Nümerik yöntem ve metodoloji detaylı olarak açıklanmıştır. Nümerik yöntemin sonuçları farklı deneyesel sonuçlar ile kıyaslanarak doğrulanmıştır. Ayrıca nümerik çözümlerin hassasiyeti, çözüme en fazla etki eden kontrol parametreleri ile sınanmıştır.

Anahtar Kelimeler: Hesaplamalı Akışkanlar Dinamiği, Küt Cisim Aerodinamiği, Ayrık Girdap Metodu

Dedicated to my family

ACKNOWLEDGEMENTS

First and foremost, I would like to thank to my supervisor, Prof. Dr. Özgür Kurç for his guidance, advices and patience in the preparation and completion of this thesis.

I also would like to thank to my wife Özlem Yalçın and my son Tibet Yalçın for their moral supports and encouragements.

Last but not the least, I would like to thank to my father Necdet Yalçın, my mother Nuriye Yalçın, and my brother Başak Yalçın for being with me in tough times of my life.

TABLE OF CONTENTS

x

LIST OF TABLES

TABLES

LIST OF FIGURES

LIST OF ABBREVIATIONS

CIC   Cloud in Cell

CFD   Computational Fluid Dynamics

DVM   Discrete Vortex Method

Exp   Experimental

FFT   Fast Fourier Transform

FV   Finite Volume

Re   Reynolds Number

RMS   Root Mean Square

RVM   Random Vortex Method

St   Strouhal Number

CHAPTER 1

INTRODUCTION

Understanding of the flow field over bluff bodies has major importance in the field of structural engineering. Flexible structures such as skyscrapers, long span suspension and cabled bridges are highly susceptible to wind action. The catastrophic failure of Tacoma Narrows suspension bridge (1940) accompanied the need of better understanding of wind-structure interaction, and after that tragic event, this area called the attention of researchers. It was later found out that the main reason of this collapse was torsional flutter instability. Therefore, understanding and quantifying the structural response of flexible structures to aerodynamic forces plays an important role during the structural design of such structures.

Experimental studies have been provided valuable insights to the researchers in understanding various important phenomena of fluid dynamics such as flutter, flow separation, complex wake formation and vortex structures for many years. On the other hand, thanks to the advances in computer technology for past four decades it has been possible to use mathematical or numerical models for simulating a fluid flow practically and there have been numerous studies about validation of those models with sufficiently consistent results. However, the challenging task has been the generalization of the numerical solution to wide variety of body shapes due to the complex nature of fluid flow.

Discrete Vortex Method (DVM) is one of the widely used numerical models in Computational Fluid Dynamics (CFD). Although relatively new compared to conventional Eulerian grid-based numerical techniques, it provides advantages of fast computational performance with accuracy and easy implementation. It has been also used in various fluid flow problems. The studies in the literature have been mostly

focusing on accuracy, computational effort and its use in different engineering problems. The model configuration may differ greatly from one study to another in terms of time integration scheme, convection and diffusion procedures, potential flow solution algorithm and, as a result, model parameters. Therefore, generalization of numerical solution to different flow problems becomes challenging.

1.1. Literature Review

1.1.1. Bluff Body Aerodynamics

It is interesting to note that there has been a rapid change in car design over a century. The early generations had rectangular parts and they had sharp edges along movement direction. Later, when it was possible to produce higher speed vehicles, engineers tend to reduce the resistance to the air flow on cars because the higher resistance would lead to higher fuel consumption and very poor aerodynamic performance (Hucho & Sovran, 1993). The solution was simply the curved geometries which would make airflow possible to follow contour of the car body. In many applications of aerodynamics, engineers have been looking for the ways to reduce drag forces and to control lift forces on the bodies such as wings of an airplane and wind turbine blades. However, the geometries like sharply changing surfaces, circular sections are inevitable because of their simplicity in use or architectural issues. The term "Bluff Body" refers to a body immersed in a flow separated along the large portion of the surface. Such separated flows differ considerably from streamlined bodies in terms of aerodynamic characteristics and conventional numerical techniques are not likely to handle the representing large, separated flows and unsteady wake.

The studies of Karman (1912) and Kirchhoff (1869) have begun a new era of bluff body flow modelling and they have been in the center of further theoretical developments. Kirchhoff developed a model by making use of Helmholtz's free streamline method on the flow around flat plate. His model was able to capture some important features of the bluff body flows such as flow separation and formation of shear layers represented as surfaces of discontinuity. The wake model was only

2

applicable on steady flow which is very rare in nature. Although today it is very well-known fact that flow pattern is highly dependent on type of flow (i.e. Reynolds number), geometry and orientation of the bodies, one of the common features of bluff body flow is periodic vortex shedding from the alternating edges with regular wake pattern. This phenomenon was named as "Karman Vortex Street" after von Karman's research (1912).

Viscous actions are to form vorticity and the amount of vorticity is mainly attributable to the size of the boundary shear layer (i.e. thickness). Therefore, one can make an inference that bluff body flows are mainly characterized by a system of vortex cloud. Importance of viscous actions was fully presented by Reynolds' experimental study (1883). After his study, it has been possible to predict flow condition (laminar or turbulent) with non-dimensional value of Reynolds number which is fundamentally a measure of ratio of inertial forces to viscous forces. In addition to his study, Strouhal (1878) investigated the vortex shedding on a circular cylinder and expressed the shedding frequency with dimensionless quantity, now widely known as Strouhal number. Findings from his experimental study showed that the number was nearly constant within a range of Reynolds number. On the other hand, significance of this non-dimensional quantity has emerged more clearly in structural engineering design after failure of Tacoma Bridge. During the formation and shedding of vortices, strong pressure fluctuations occur. If dominant frequency of alternating forces become close to the natural frequency of a structure, resonance response may occur. This case is commonly referred to critical speed effect (Morgenthal, 2000). Moreover, physical aspects of vortex shedding mechanism on a particular body geometry and flow conditions have importance in determining serviceability condition and its contribution to fatigue. Therefore, the phenomenon has been on the top interest in the field of bluff body aerodynamics for nearly a half century.

In early wind tunnel experiments and numerical studies in the field of bluff body aerodynamics, flow field around the most common bluff shapes such as circular, rectangular, and trapezoidal sections were investigated since they have been

frequently preferred in the civil engineering structures. The attention was paid to the possible effects on flow field and aerodynamic properties. First of all, the geometry itself should be considered separately from other parameters, since each shape exhibits different characteristics of flow fields. Considering sharp edged bodies, flow separation takes place most possibly on the corners; however, it significantly depends on Reynolds number for circular cylinders (Schlichting, 1979). For very wide range of Reynolds number for the flow over a rectangular section, base pressure and force coefficients show slight changes (Bearman & Trueman, 1972). Similarly, Okajima (1982) studied the flow around rectangular cylinders of Reynolds number varying between 70 and 20.000 and the results from wind tunnel tests showed that Strouhal number was in between 0.12 and 0.14. On the other hand, flow fields vary from each other with different aspect ratios and angle of incidence as investigated experimentally and numerically on the rectangular prisms (Bearman & Trueman, 1972), (Norberg, 1993), (Taylor & Vezza, 1999).

Lee (1974) and Bearman & Trueman (1972) investigated experimentally the effect of turbulence on aerodynamic forces and pressure distribution along a square section. Introducing turbulence to the stream increased the wake pressure (i.e. reduce drag force) and reduced the lift fluctuations by changing shear layer and vortex formation patterns. On the other hand, the most noticeable effect of turbulence has been seen at low angle of attack as Vickery (1966) investigated smooth and turbulent flow over square prism at various orientations.

The rigidity of a body against an oncoming flow reveals more complicated flow field. If a complete rigidity is not satisfied, in that case the body deforms and vibrates under the effect of aerodynamic forces. Therefore, the body undergoes different pressure distributions and forces due to fluid-structure interactions, namely aeroelasticity. Aeroelastic phenomena are mainly treated as subjects of bluff body aerodynamics and the reason may come from the fact that the most of body in structural engineering have blunt shapes. To better understand the phenomena, it is helpful to classify the predominant effects. One classification was proposed by Naudascher and Rockwell

(1994). They distinguish three types of flow-induced excitation: Extraneously induced excitation, instability induced excitation and movement induced excitation. In reality, flow induced vibrations can include one or combination of them.

1.1.2. Discrete Vortex Method

Vortex particle method is based on discretization of vorticity field in a cloud of discrete vortices. In each time step, position and velocity of the particles are estimated in convection process based on velocity-vorticity relationship. The method outstands on vortices, since a typical flow contains vorticity in a small portion of it. Because of not requiring a mesh, Discrete Vortex Method (DVM) can provide better resolution of the high vorticity areas and separated regions (Lewis, 1991). Therefore, direct advantage will be savings in storage and computational performance, and many difficulties experienced in grid-based numerical methods such as numerical diffusion, numerical instabilities due to excessive grid refinement and necessity of fine meshing near the wall region are avoided (Taylor I. J., 1999).

The method has been in development since the pioneering work of Rosenhead (1931). His study was the first real dynamical vortex simulation which investigated Kelvin-Helmholtz instability of a surface of discontinuities. The primary objective of the study was to simulate the shear layer by point vortices and the deformation of the vortex sheet via convection of vortices with a simple Eulerian integration. A relatively new and powerful computational technique, surface vorticity boundary integral method for potential flow proposed by E. Martensen (1959) became the foundation of surface vorticity modelling. On the other hand, the viscosity which has a significant effect of the vortex shedding has been missing until the first viscous algorithm named as random walk method (RVM) for discrete vortex method has been originally proposed by Chorin (1973). Chorin applied this technique to flow around cylinders and flat plates. Hald (1984) and Goodman (1987) studied the consistency of the algorithm. Chang (1988) integrated Runge-Kutta time stepping scheme to the

algorithm. In analogy to Chorin's algorithm, Porthouse & Lewis (1981) developed a random walk technique for vortex cloud modelling.

Random walk algorithm is easily adoptable and can be used for complex body geometries. In principle, random displacements are given to the vortices in order to simulate diffusion by conserving the total circulation. Therefore, diffusion equation is solved in a statistical manner and flow solution is noisy due to statistical errors. The noise level in the solution may prevent obtaining reasonable accuracy and understanding the effect of control parameters. Fogelson and Dillon (1993) emphasized the necessity of smoothing the random walk solution and they concluded that large number of vortices is required to obtain an accurate solution. On the other hand, Roberts (1985) demonstrated that the choice of initial conditions is very important while using RVM. He also proved that the accuracy of RVM decreases for increasing Reynolds number for constant number of vortex blobs.

With the help of Langrangian nature of discrete vortex method, computational effort can be mostly performed in the regions where important fluid action takes place. Velocity field can be obtained at any instant by using Biot-Savart law integral on the contrary to Euler scheme which requires information at the uninterested regions (Lewis, 1991). Surface of a body acts like a source of vorticity creation and vortices are shed from the source panels modelled along the surface. Since total number of vortices is increased by the number of source panels at each time step, computational economy provided by DVM may not last long if excessive number of vortices is utilized. Convection calculations requires $O(N^2)$ operations where N stands for total number of vortices. The simplest way to minimize the operation counts without introducing a considerable error is vortex merging procedure (Spalart, 1988). With this procedure, pairs of vortices within the close proximity are merged into single vortex particle. The new vortex particle is placed at centroid of the old ones and total circulation is conserved by summing circulations of pair vortices.

Use of grid system for convection calculations of vortex method provides considerable reduction in operation counts. One of the very well-known schemes is Cloud-in-cell (CIC) method. Formerly, a new convection scheme for Langrangian vortex method which is based on re-distribution of discrete vortices onto a fixed grid system was proposed by Christiansen (1973). Later the method has been developed and applied to vortex cloud modelling of incompressible and rotational flows by various researchers (Spalart, 1988), (Smith & Stansby, 1988), (Stansby & Dixon, 1983), (Leonard, 1980). Basically, in this method a cloud of vortices within a square or rectangular grid cell is replaced by four vortices located at cell corners. Smith and Stansby (1988) have shown the advantages of the method in terms of efficiency and precision. They reported that operation counts reduce from $O(N^2)$ to $O(M\log M)$ where M is total number of grids. Similarly, Spalart and Leonard (1981) have used grid system to compute longer distance interactions with grouping vortices in grid cells.

1.2. Objective and Scope

The objective of this study is to develop a numerical tool to simulate 2-dimensional incompressible and viscous air flow around bluff bodies by using Langrangian vortex method with viscous formulation of Random Walk technique. Moreover, parametric studies are conducted to examine the sensitivity of the input parameters on stability and accuracy of the solutions.

A 2D Discrete vortex algorithm is written in C++ programming language. The code has been developed by (Kaya, 2012). The results of the program are validated by comparing its results with several experimental results. In the parametric studies, the effect of time step size, panel size, and grid size which are determined to inhibit more significant effect on the solutions among all other parameters, are examined. Both validation and parametric studies have been conducted to simulate laminar and unsteady air flow of moderate Reynolds number (10.000 – 30.000) around rectangular prisms and a bridge deck section. The rigid blunt bodies which are fixed in space, have been immersed to air flow having constant velocity at free stream.

CHAPTER 2

NUMERICAL METHODOLOGY

The fundamentals of two-dimensional discrete vortex method algorithm for unsteady, incompressible, and viscous air flow used in the thesis are discussed. Initially, the evolution of governing equations by using velocity-vorticity relationship is given in terms of material derivative form. Vorticity transport equation is divided into sequential convection and diffusion processes by using operator splitting method. Velocity field is estimated by Biot-Savart law followed by random walk technique to simulate diffusion of vorticity. A boundary integral equation is used to model surface vorticity in the potential flow analysis. Besides the theoretical aspects of discrete vortex method, the computational sequence is explained.

2.1. Governing Equations

Two-dimensional incompressible flow is governed by continuity and full viscous Navier-Stokes equations as given:

$$\nabla . \boldsymbol{u} = 0 \tag{2.1}$$

$$\frac{\partial \boldsymbol{u}}{\partial \boldsymbol{t}} + \boldsymbol{u} . \nabla \boldsymbol{u} = -\frac{1}{\boldsymbol{\rho}} \nabla \boldsymbol{p} + \boldsymbol{\nu} \nabla^2 \boldsymbol{u} \tag{2.2}$$

where $\boldsymbol{t}$ is time, $\boldsymbol{u}$ is flow velocity, $\boldsymbol{\rho}$ is the fluid density, $\boldsymbol{p}$ is pressure, and $\boldsymbol{\nu}$ is the kinematic viscosity of the fluid. In vortex method, conventional form of the equations is redefined by using velocity-vorticity formulation as given:

$$\boldsymbol{\omega} = \nabla \times \boldsymbol{u} \tag{2.3}$$

By taking curl of the equation (2.1), following vorticity equation in Lagrangian form is obtained:

$$\frac{\partial \boldsymbol{\omega}}{\partial t} = (\boldsymbol{\omega}.\nabla)\boldsymbol{u} - \boldsymbol{\omega}(\nabla.\boldsymbol{u}) + \frac{\nabla\boldsymbol{\rho} \times \nabla\boldsymbol{p}}{\rho^2} + \boldsymbol{\nu}\nabla^2\boldsymbol{\omega} \qquad (2.4)$$

For an incompressible fluid, the term $\nabla\boldsymbol{\rho}$ is zero and therefore baroclinic term vanishes from the equation. The term $\boldsymbol{\omega}(\nabla.\boldsymbol{u})$ is zero from the continuity equation. First term of the right-hand side of the equation represents stretching and tilting of vortex tubes due to velocity gradient. Considering two-dimensional flow, this term also vanishes. Hence, the equation (2.4) can be re-written in material derivative form as given,

$$\frac{D\boldsymbol{\omega}}{Dt} = \boldsymbol{\nu}\nabla^2\boldsymbol{\omega} \qquad (2.5)$$

To solve equation (2.5), Chorin (1973) proposed the operator splitting method which applies the sequential rather than simultaneous convection and diffusion of vorticity. The convection process is solved according to the inviscid form of equation (2.5) as given:

$$\frac{D\boldsymbol{\omega}}{Dt} = \boldsymbol{0} \qquad (2.6)$$

then, diffusion process is solved by including viscous term in the Navier-Stokes equation which is:

$$\frac{\partial \boldsymbol{\omega}}{\partial t} = \boldsymbol{\nu}\nabla^2\boldsymbol{\omega} \qquad (2.7)$$

2.2. Determination of Velocity Field

The continuity equation (2.1) can be satisfied by using a stream function $\boldsymbol{\psi}$ such that:

$$\boldsymbol{u} = \nabla \times \boldsymbol{\psi} \qquad (2.8)$$

If the equation (2.8) is substituted in velocity-vorticity equation (2.3), following Poisson equation can be obtained

$$\nabla^2 \psi = -\omega \qquad (2.9)$$

The common approach to solve the Poisson equation is using Green's function and 2D velocity field on x-y plane for unbounded flows can be obtained by well-known Biot-Savart law as follows,

$$u = \boldsymbol{K} * \omega = -\frac{1}{2\pi} \int \boldsymbol{K}(x - y)x\,\omega\,dy + U_0 \qquad (2.10)$$

where U_0 is the solution of homogenous Poisson equation and $\boldsymbol{K}$ is the Biot-Savart kernel or the velocity kernel given by

$$\boldsymbol{K}(x - y) = \frac{(x - y)}{|x - y|^2} \qquad (2.11)$$

2.3. Surface Vorticity Model for Potential Flow Analysis

In surface vorticity model, the body immersed in a uniform flow W_∞ is discretized with finite number of surface vorticity panels whose strength is initially unknown as illustrated in Figure 2-1. The boundary layer is simplified to a vortex sheet of strength $\gamma(s_n)$. The velocity dq_{mn} at point s_m induced by vorticity element $\gamma(s_n)ds_n$ located at s_n may then be expressed from Biot-Savart law as follows,

$$dq_{mn} = \frac{\gamma(s_n)ds_n}{2\pi r_{mn}} \qquad (2.12)$$

The velocity components of dq_{mn} in x-y plane parallel to s_m can be calculated according to the following equation

$$dv_{mn} = \frac{1}{2\pi}\left\{\frac{(y_m - y_n)\cos\beta_m - (x_m - x_n)\sin\beta_m}{(x_m - x_n)^2 + (y_m - y_n)^2}\right\}\gamma(s_n)ds_n \qquad (2.13)$$
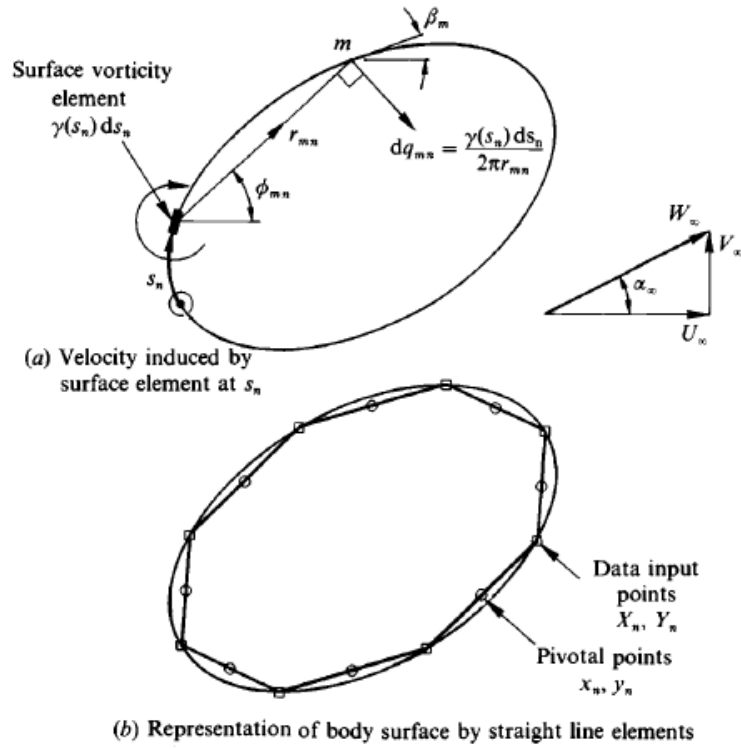
Figure 2-1. Discrete surface vorticity model for a two-dimensional body *(Lewis, 1991)*

Martensen (1959) proposed a boundary integral equation for the potential flows given as:

$$-\frac{1}{2}\gamma(s_m) + \oint k(s_m, s_n)\gamma(s_n)ds_n + W_\infty \cos(\alpha_\infty - \beta_m) = 0 \qquad (2.14)$$

where k is the coupling coefficient given by following equation,

$$k(s_m, s_n) = \frac{1}{2\pi}\left\{\frac{(y_m - y_n)\cos\beta_m - (x_m - x_n)\sin\beta_m}{(x_m - x_n)^2 + (y_m - y_n)^2}\right\} \qquad (2.15)$$

For a finite number of surface vortices as illustrated in Figure 2-1, the coupling coefficient K can be written as

12

$$K(s_m, s_n) = \frac{\Delta s_n}{2\pi} \left\{ \frac{(y_m - y_n)\cos\beta_m - (x_m - x_n)\sin\beta_m}{(x_m - x_n)^2 + (y_m - y_n)^2} \right\}$$
$$= k(s_m, s_n)\,\Delta s_n \qquad (2.16)$$

It should be noted that the coupling coefficient for self-induced velocity ($m = n$) is indeterminate, since both numerator and denominator terms are zero. It can be assumed to be zero for body surface which is polygonal, but it would be non-zero for the curved geometries (Lewis, 1991).

2.4. Convection

In a flow field containing N particles, calculation of velocity of a single vortex element can be calculated by taking the influence of all vortices in the flow field into account. This turns out to be an operation count of O(N^2). Once the potential flow solution is obtained for $\gamma(s_m)$, velocity component at vortex element m induced by element n with a unit strength of $\Delta\Gamma_n$ can be estimated from

$$U_{mn} = \frac{1}{2\pi}\left[\frac{y_m - y_n}{(x_m - x_n)^2 + (y_m - y_n)^2} \right]$$
$$V_{mn} = -\frac{1}{2\pi}\left[\frac{x_m - x_n}{(x_m - x_n)^2 + (y_m - y_n)^2} \right] \qquad (2.17)$$

Consequently, convection velocity components at vortex m due to vortex cloud of N is given by

$$u_m = \sum_{\substack{n=1 \\ n \neq m}}^{N} \Delta\Gamma_n U_{mn}$$
$$v_m = \sum_{\substack{n=1 \\ n \neq m}}^{N} \Delta\Gamma_n V_{mn} \qquad (2.18)$$

In present study, time integration of simple forward difference scheme is used. Therefore, vortex m has the convective displacement components from initial position of a at time t$_i$ to position b at time t$_{i+1}$ is given by

$$x_{mb} = x_{ma} + u_m \Delta t$$
$$y_{mb} = y_{ma} + v_m \Delta t$$

(2.19)

The equation (2.19) represents fully Langrangian description of convection process. As stated before, every time step the number of M new particles are released to the flow field. This leads to computational expenses due to operation count of $O(N^2)$ with newly created vortices. To reduce the operation count, Eulerian grid system is commonly used for speed up of convection process. During the parametric study simulations, grid-based flow solutions with very well-known CIC scheme are also discussed beside of non-grid solutions.

CIC technique is derived from Poisson's equation for the stream function (Lewis, 1991), and convection process is applied by distributing vorticity to grid points. After constructing grid system, the discrete vortex $\Delta \Gamma_n$ located at (x_n,y_n) is splitted to the nearest cell corners with bi-linear interpolation (area weighting) as shown in Figure 2-2.
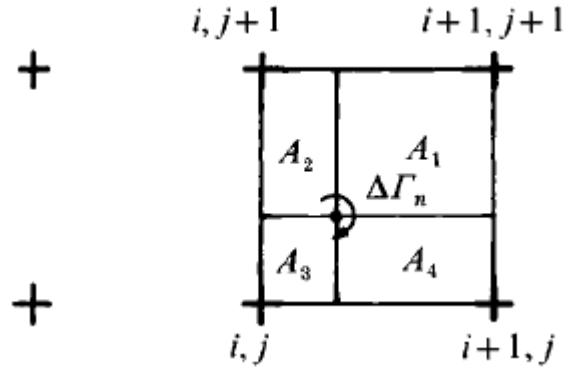
Figure 2-2. Area weightings for discrete vortex at (x_n,y_n) *(Lewis, 1991)*

The vorticity at grid point (*i,j*) is given by the accumulated vorticity after redistribution of all discrete vortices to cell corners as follows

$$\omega_{ij} = \Gamma_{ij}/A$$

(2.20)

The vortex convection velocity of vortex n can be obtained by interpolating grid velocities with area weighting procedure as given

$$
\begin{aligned}
u_n &= \sum_{p=1}^{4} u(p) A_p / A \\
v_n &= \sum_{p=1}^{4} v(p) A_p / A
\end{aligned}
\tag{2.21}
$$

2.5. Diffusion

The diffusion equation (2.7) can be expressed in terms of polar coordinates as following equation,

$$
\frac{\partial \omega}{\partial t} = \nu \left\{ \frac{\partial^2 \omega}{\partial r^2} + \frac{1}{r} \frac{\partial \omega}{\partial r} \right\}
\tag{2.22}
$$

The well-known solution is obtained by using Green's function (Batchelor, 1970) as follows,

$$
\omega(r, t) = \frac{\Gamma}{4\pi\nu t} e^{(-r^2/4\nu t)}
\tag{2.23}
$$

The random walk technique developed by Porthouse and Lewis (1981) is based on a stochastic approach to the solution of this equation in such a way that a particle (i) is subjected to a random walk with zero mean and variance $2\nu\Delta t$ by following equation,

$$
x_i^{k+1} = x^k + r_p
\tag{2.24}
$$

where x^k is the position of the particle after k^{th} convection steps and r_p is a random vector satisfying the equation (2.25). The radial (Δr) and circumferential diffusive ($\Delta\theta$) displacement of any particle for time step size of Δt is estimated by following equation

$$\Delta r = \sqrt{4\nu\Delta t \ln\frac{1}{P}}$$

(2.25)

$$\Delta\theta = 2\pi\emptyset$$

where P and $\emptyset$ are uniform random numbers between 0 and 1 of a uniform probability distribution. The diffusive displacement and position of a particle by applying random walk displacements for 10,000 time-step (assuming $\nu = 1$ and $\Delta t = 1$) are illustrated in Figure 2-3.

(a)   (b)
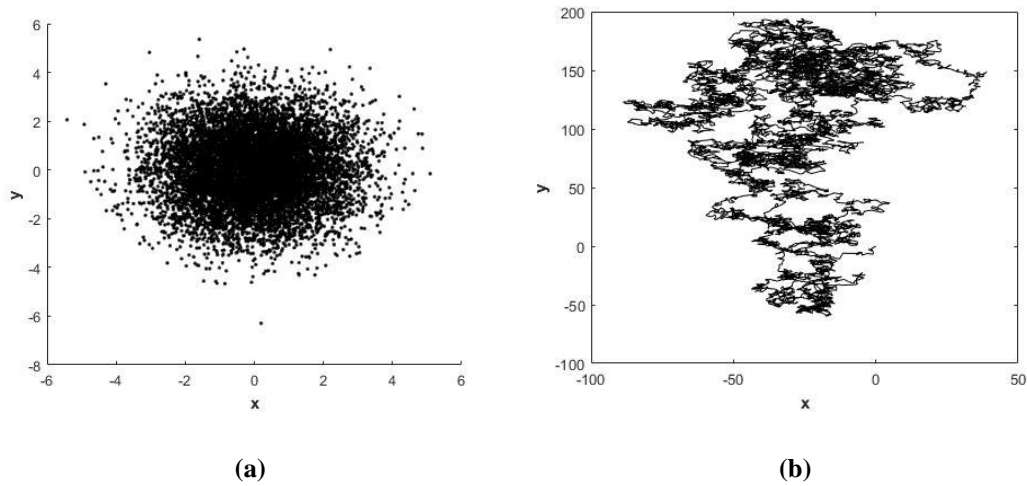
Figure 2-3. The diffusive displacement (a) and position (b) of a particle

2.6. Surface Pressure and Force Calculation

Once the diffusion and convection have been solved in the equation (2.2), Navier-Stokes equations reduced to following equation with tangential vector of the body surface under the assumption of a stationary body,

$$-\frac{1}{\rho}\frac{\partial p}{\partial s} = \nu\frac{\partial\omega}{\partial n}$$

(2.26)

16

A numerical expression can be derived from the equation (2.26) for the change in surface pressure over the surface element n in a time step size of Δt,

$$\Delta p_n = -\rho \frac{\gamma(s_n)\Delta s_n}{\Delta t} = -\rho \frac{\Delta \Gamma_n}{\Delta t} \tag{2.27}$$

Consequently, the equation (2.27) can be integrated to estimate the surface pressure (p_i) at any point relative to datum value p_1 which is initially zero from where the integration of (2.26) starts for numerical convenience,

$$p_i = p_1 + \sum_{n=1}^{M} \Delta p_n \tag{2.28}$$

Non-dimensional aerodynamic features are also calculated for comparison of the results with those corresponding to other numerical and experimental studies. The pressure coefficient is given by,

$$C_P = \frac{p - p_\infty}{\frac{1}{2}\rho W_\infty^2} \tag{2.29}$$

where p_∞ is free stream fluid pressure. The average surface pressure is given by,

$$C_{P_{avg}} = \frac{p_{avg} - p_\infty}{\frac{1}{2}\rho W_\infty^2} \tag{2.30}$$

where p_{avg} is the average surface pressure. Lift (L) and drag (D) forces can be estimated by integration of the pressure over the surface in cartesian coordinates. Therefore, lift and drag force coefficient can be estimated as follows,

$$C_L = \frac{L}{\frac{1}{2}\rho W_\infty^2 \ell_L} \tag{2.31}$$

$$C_D = \frac{D}{\frac{1}{2}\rho W_\infty^2 \ell_D} \qquad (2.32)$$

where ℓ_L and ℓ_D are characteristic length for lift and drag forces, respectively. Another dimensionless quantity is Strouhal Number (St) which is a measure of vortex shedding frequency is given by,

$$St = \frac{f\,l}{W_\infty} \qquad (2.33)$$

where f is dominant frequency obtained from force signal spectra and l is characteristic length.

2.7. Vortex Shedding

Surface vorticity is created by discretizing solid body surface into straight source panels. In each time step, vorticity sheets $\gamma(s_n)\Delta s_n$ are created and released to free stream at vortex creation points having the normal distance of $\varepsilon = \Delta s_n/2$ (Spalart, 1988) to the mid-point of source panel (Figure 2-4).
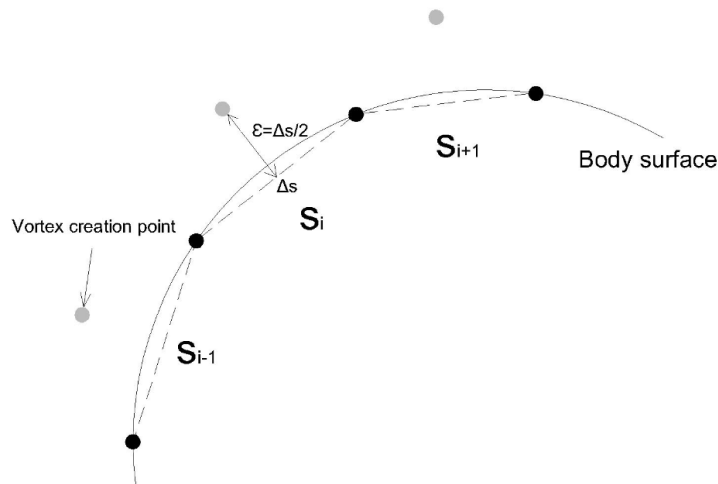
Figure 2-4. Vortex shedding

2.8. Vortex Particles Within Close Proximity

Applying Biot-Savart law for any two vortex particles within the close proximity may result in excessive velocity contribution of mutual convection. In an exaggerated manner, if the distance of two particles r_{mn} becomes close to zero, induced velocity will approach to infinity from equation (2.12). In order to limit mutual convection velocities for the nearby vortices, Rankine Core model is implemented in the numerical algorithm. In this model, the convection velocities are modified for the special cases when distance of two particles is smaller than core radius $d = \Delta s_n/4$ as recommended by Spalart (1988). On the other hand, the equation (2.17) is valid for other instances. Velocity components at particle m induced by particle n having unit strength and located at a distance smaller than d are estimated as follows,

$$U_{mn} = \frac{y_m - y_n}{2\pi\, d^2}$$

$$V_{mn} = -\frac{x_m - x_n}{2\pi\, d^2}$$

(2.34)

A representative relationship between induced velocity and distance of any two particles is illustrated at Figure 2-5. The dashed line is the case of Biot-Savart Law without applying Rankine Core Model.
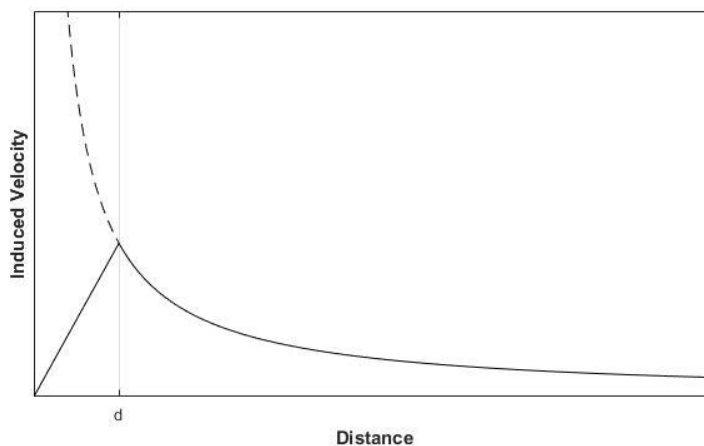
Figure 2-5. Induced velocity with respect to distance

19

2.9. Particle Merging and Deletion

Vortices are created at each time step, and number of particles in the domain increases by the panel number. In order to achieve computational economy, control of the number of vortices is required especially for the simulations without grid system. Accordingly, Deffenbaugh and Marshall (1976) have come up with a simple merging device in order to reduce the number of vortices. It has been used to merge pairs of vortices near the wall region. Similarly, a merging procedure is constructed in this study such that vortex pairs within the limiting distance are merged into a single vortex and released at vortex centroid with conserving the total circulation. While providing computational economy, the solution is aimed to have negligible effect due to merging. As a result of the experience obtained from the simulations, merging procedure is followed at every 6-time steps and the limiting distance is selected to be the half of the core radius d. The changes in the average pressure distribution and forces due to merging are less than 1% and 0.1%, respectively.

Vortices near the wall region are possible to cross surface followed by convection and diffusion process. Chorin (1973) recommends those vortices to be bounced back to the free stream. On the other hand, Porthouse (1983) recommends those should be deleted during the next convection process. Besides of providing computational economy by containing the number of vortices, deletion procedure is appropriate for viscous flow (Spalart, 1988). Therefore, vortex particles crossing the wall are contained for following convection process and then deleted in order to ensure vorticity conservation in the present study.

2.10. Computational Scheme

The present DVM algorithm is developed by C++ programming language. The computational scheme of the present study is illustrated in Figure 2-6. The data points of the body surface and input parameters are constructed prior to model run. Therefore, the first step of the computational scheme is reading of input data. Depending on the data points, the panels are defined in terms of orientation and the coordinates of pivotal

points. The coupling coefficient matrix K is then constructed according to the panel information. Since there are no active vortices in the domain at the beginning, the equation 2-14 is solved for unknown discrete surface vorticity with only free stream velocity. Time iterative procedure starts with shedding of the new vortices from the creation points as illustrated in Figure 2-4, then velocity of each particle is calculated. By applying simple forward difference scheme, convective and random walk displacement of each particle is estimated respectively. The vorticity strength of each panel is estimated for the next time step. Finally, particle merging and deleting procedure is followed. Finally, pressure and force coefficients are calculated. The next time step is started by shedding of the newly created vortices.
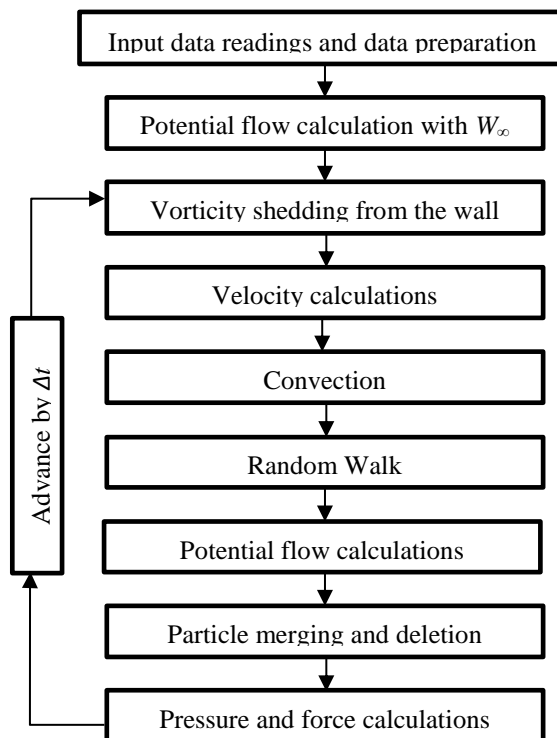
Figure 2-6. Computational scheme

21

CHAPTER 3

VALIDATION STUDIES

Discrete Vortex Method algorithm with viscous diffusion formulation of Random Walk Method is examined on unsteady flow over several bluff bodies by comparing aerodynamic properties obtained from 2D DVM solution with the investigations conducted by other researchers. Due to wide use of rectangular geometries in civil engineering structures, DVM algorithm is examined on flow over rectangular sections. Initially, DVM solution is analyzed for flow around square section with Reynolds Number of 17,600 in terms of mean and fluctuating force coefficients, pressure distribution and frequency of the vortex shedding by comparing with the experimental results obtained from literature. Then, the validation studies are extended to rectangular sections with Reynolds Number of 13,000 in order to examine DVM for varying aspect ratios. The results are compared with an experimental study in terms of mean drag coefficient and Strouhal Number. Moreover, the accuracy of DVM is conducted for the effect of changing shapes in smaller scale and flow solution for square prism with sharp and chamfered corners are performed. The results are then compared with the experimental study conducted by Tamura et al. (1999) in terms of mean force coefficients and Strouhal Number. Finally, the validation studies are completed by examining DVM solution for flow around a long span suspension bridge deck section.

In all simulations, convection calculations are performed by introducing a grid system with cell-in-cell interaction method (CIC) in order to increase computational performance. The length scaled parameters which are panel size (Δs), vortex shedding distance from the wall (ε) and vortex core radius (d) are related as follows: $\varepsilon=\Delta s/2$, $d=\Delta s/4$. The computational domains are limited to 5 times of D (width) and 20 times of B (length) of the sections.

3.1. Flow Over Square Section

DVM algorithm is examined on uniform flow having 10 m/s free stream velocity (U) over a square section with Re of 17600. The calculation is performed at non-dimensional time step of 0.01 and surface of the square section is discretized into 200 equal length panels. Grid system is used in the convection calculations, and grid spacing is selected as 5 % of side length in each direction.
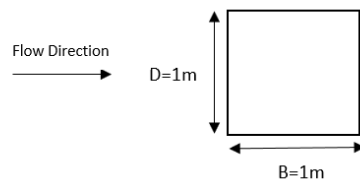
Figure 3-1. Square section

As a result of the flow field solution, the regular vortex shedding at alternating downstream corners is obtained. Particle distribution at non-dimensional time (tU/D) of t*=137 is illustrated in Figure 3-2 and the vortex street on the wake can be clearly seen.

Figure 3-2. Flow at non-dimensional time 137 for Re = 17600

24

A summary of comparison of aerodynamic properties are presented in Table 3-1. In general, DVM results show good agreement with the experimental results in terms of mean (C_{Davg}) and standard deviation (C_D') of drag coefficient. By performing Fast Fourier Transform algorithm on the lift force signal, the vortex shedding frequency is found to be 2 Hz (see Figure 3-3) with corresponding St of 0.14 which is slightly higher than the experimental values. On the other hand, the estimated standard deviation of lift force fluctuation (C_L') has the error of 17% - 23% with respect to experimental results.

Table 3-1. *Comparison of aerodynamic properties of DVM solution of flow over square section*

Study	Re	C_{Davg}	C_D'	C_L'	St
DVM (Present)	$1.8*10^4$	2.11	0.19	1.02	0.14
Lee (1974) (Exp)	$1.8*10^5$	2.07	0.17	1.23	0.12
Norberg (1993) (Exp)	$1.3*10^4$	2.16	-	-	0.13
Vickery (1966) (Exp)	$4.0*10^4 - 1.6*10^5$	2.03	-	1.32	0.12
Taylor & Vezza (1999) (DVM)	$2.0*10^4$	2.38	-	-	0.13
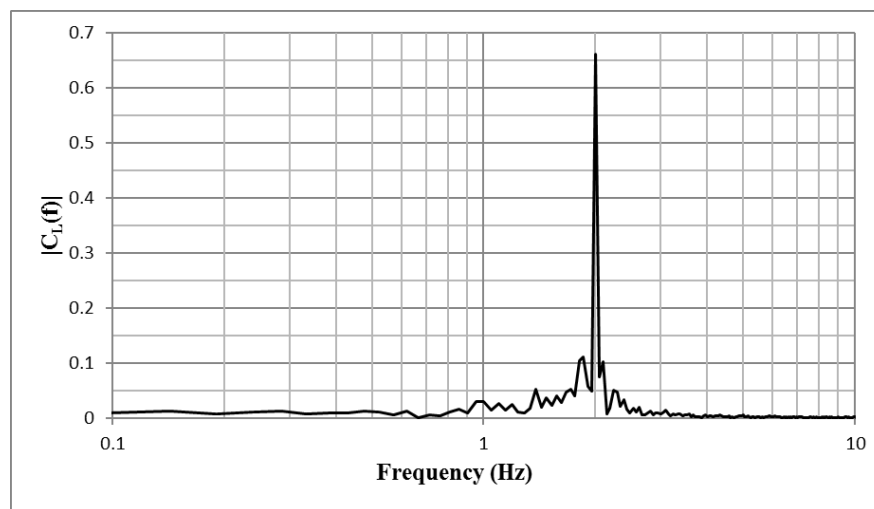
Figure 3-3. Spectra of lift coefficient (C_L) for flow over square section with Re 17600

The pressure distributions obtained from DVM simulations are compared with experimental results (Lee, 1974). Mean and standard deviation of pressure coefficient distributions are presented in Figure 3-4 and Figure 3-5, respectively. It can be seen that present DVM result and the experimental values are well matched along the leading and wake stream faces (AB and CD) in terms of mean pressure distribution. Moreover, it is overestimated around 20% for streamwise faces (AD and BC). On the other hand, standard deviation distributions of pressure coefficient obtained from DVM simulation compare very well with the experimental results (Lee, 1974). Considering the significant pressure fluctuations taking place on the side walls parallel to free stream and complex wake formation behind the body, it can be concluded that DVM algorithm very well simulates pressure oscillation with high resolution based on the present model inputs.
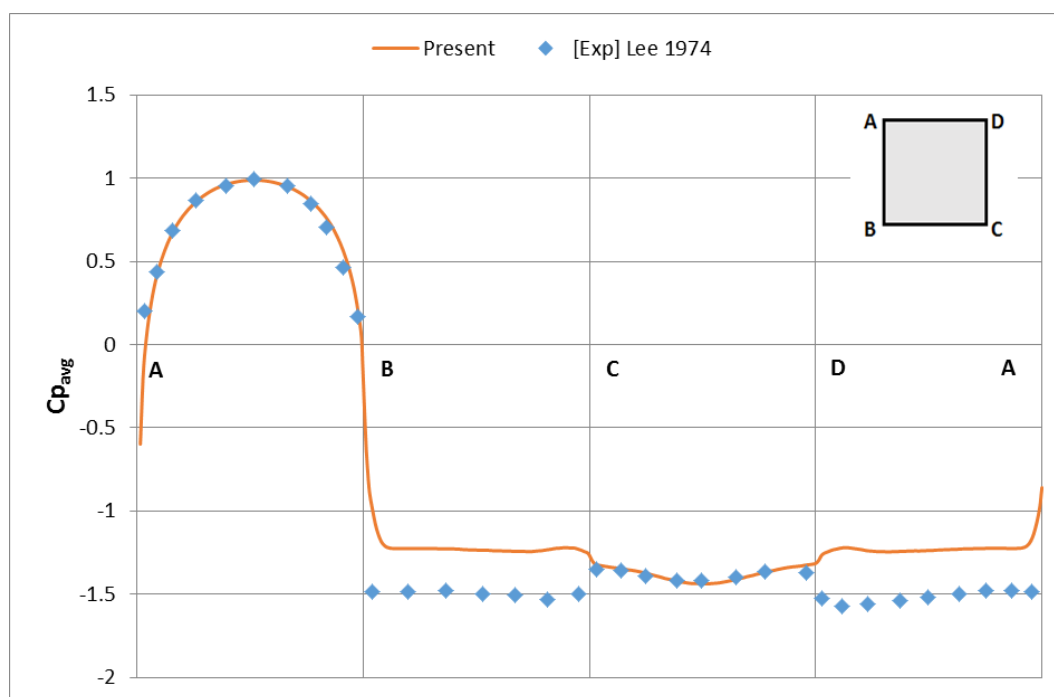
Figure 3-4. Distribution of mean pressure coefficient (C_{Pavg}) for Re 17600

26
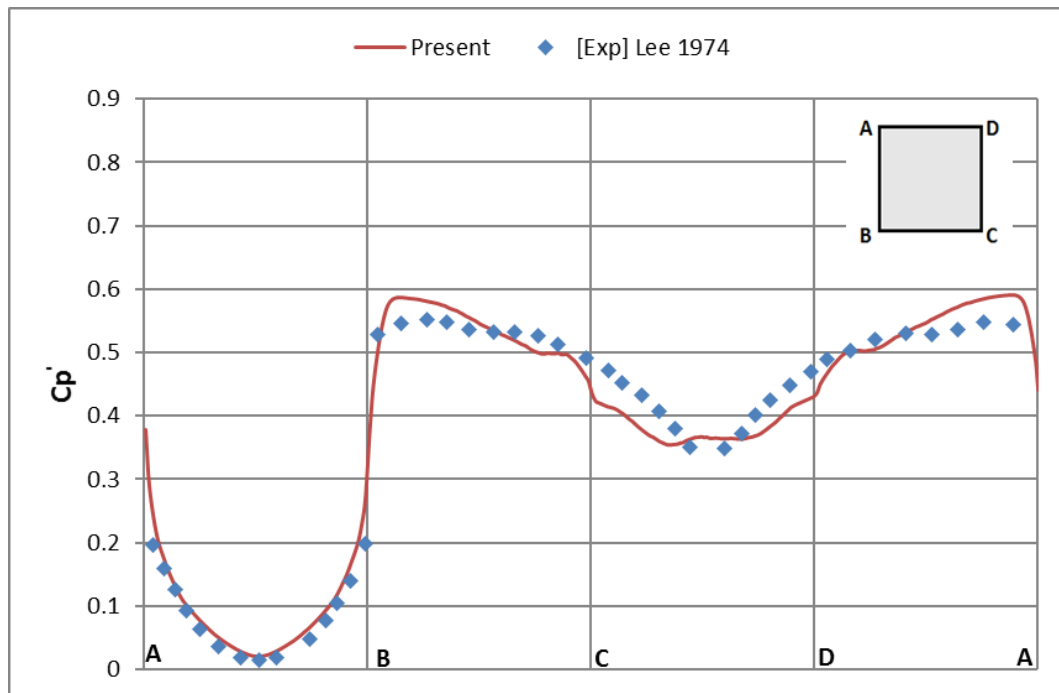
Figure 3-5. Distribution of standard deviation of fluctuating pressure coefficient (C_P')

3.2. Flow Over Rectangular Cylinders with Different Aspect Ratio

Flow over rectangular cylinders having different aspect ratios is simulated by using DVM algorithm and compared with experimental results (Norberg, 1993). Aspect ratio is defined as the ratio of side length along flow direction (B) to side length perpendicular to flow direction (D) as shown in Figure 3-6. Aspect ratio of cylinders in present simulations is chosen between 0.3 and 2.5 similar to the experimental study conducted by Norberg (1993) with Reynolds number of 13.000. Panel numbers used in the present simulations vary between 210 and 280.
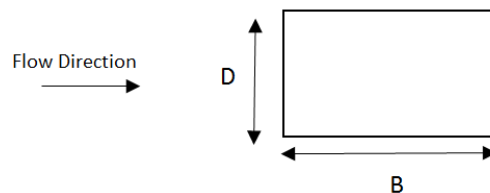
Figure 3-6. Rectangular section with aspect ratio of B/D

27

In Table 3-2 length scaled parameters and section properties are presented. DVM simulation with different aspect ratio (B/D) is denoted R following by value of the ratio.

Table 3-2. *Model Geometries and Parameters*

Section	D (m)	B (m)	Panel Number	Panel Size Δs	Shedding Distance $(\varepsilon = \Delta s/2)$	Core Radius $(d = \Delta s/4)$
R 0.3	1.00	0.33	240	0.0111	0.0056	0.0028
R 0.5	1.00	0.50	240	0.0125	0.0063	0.0031
R 0.6	1.00	0.63	248	0.0132	0.0066	0.0033
R 0.75	1.00	0.75	210	0.0167	0.0083	0.0042
R 1.0	1.00	1.00	240	0.0167	0.0083	0.0042
R 1.5	1.00	1.50	250	0.0200	0.0100	0.0050
R 1.6	1.00	1.60	248	0.0210	0.0105	0.0052
R 2.0	1.00	2.00	240	0.0250	0.0125	0.0063
R 2.5	1.00	2.50	280	0.0250	0.0125	0.0063

Results are compared with the experiment in terms of average drag coefficient (C_{Davg}) and Strouhal Number which are illustrated in Figure 3-9. Drag and lift forces with respect to non-dimensional time are presented in Figure 3-7 and Figure 3-8 respectively. It is seen that flow is fully developed and regular vortex shedding at alternating downstream corners is achieved after approximately non-dimensional time of 35 for all aspect ratios.
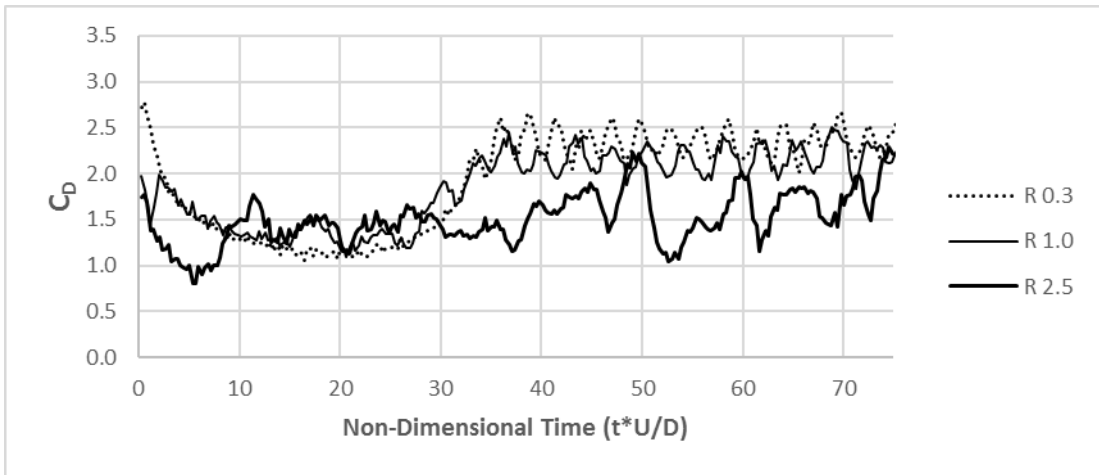
Figure 3-7. Drag coefficient
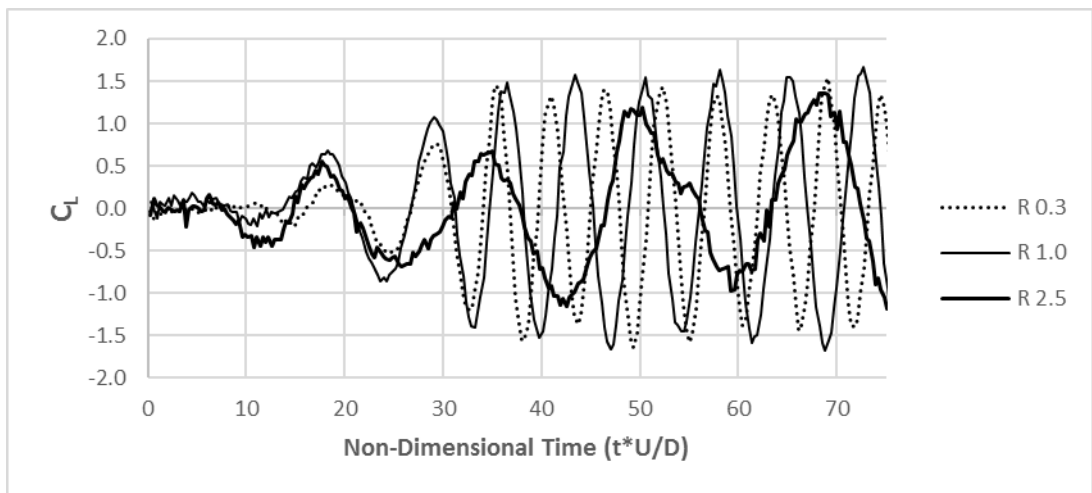
Figure 3-8. Lift coefficient
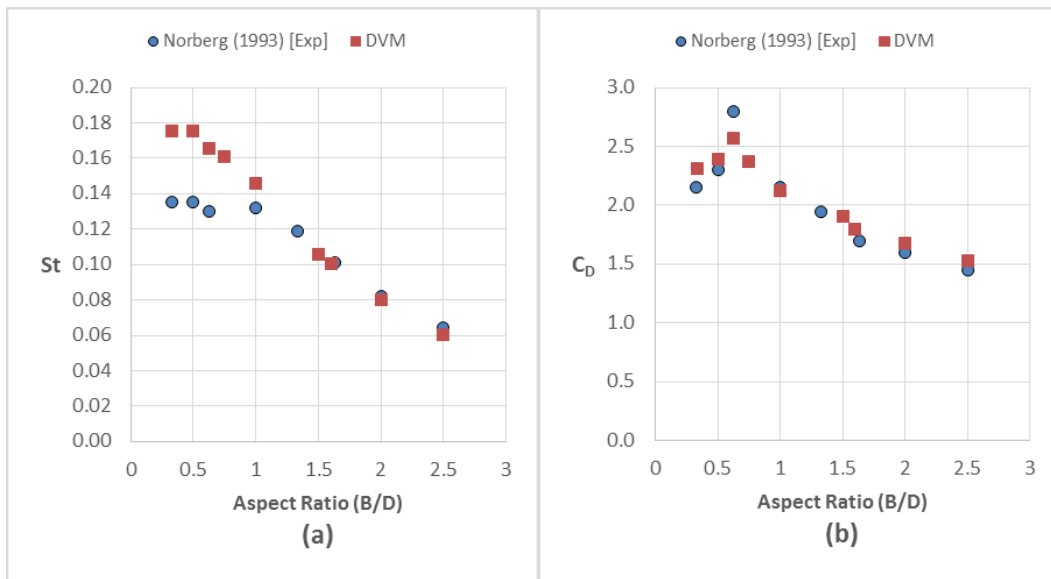
Figure 3-9. Experimental and present numerical results of St Number (a) and mean drag coefficient (b) with aspect ratio

Strouhal Number and mean drag coefficient obtained from DVM solution for different aspect ratio are presented in Figure 3-9. It is seen that DVM results show very good agreement with the experiment in the prediction of mean drag force. In addition, maximum mean drag force is obtained for rectangular section with aspect ratio of 0.63 the so called "critical section" or "golden section" in parallel with the experimental findings (Norberg, 1993), (Bearman & Trueman, 1972). According to Bearman and Trueman (1972), the high drag force is developed on the leeward face of rectangular sections and related to complex vortex formation behind the body. For the critical section, the curvature of the shear layer reaches to the upper limit which results in more suction on the wake. Flow visualization from DVM simulation with three different aspect ratios is illustrated in Figure 3-10.

On the other hand, variation of Strouhal Number with aspect ratio compares well with experiment although a general tendency to overestimation of Strouhal Number for smaller aspect ratio is seen. The reason of overestimating Strouhal Number is not clear. However, DVM tends to predict pressure distribution more consistently at the sides normal to flow direction compared to the sides parallel to the flow. Similarly, it

performs better on predicting drag coefficient than lift coefficient and therefore Strouhal Number.

(a)

(b)

(c)
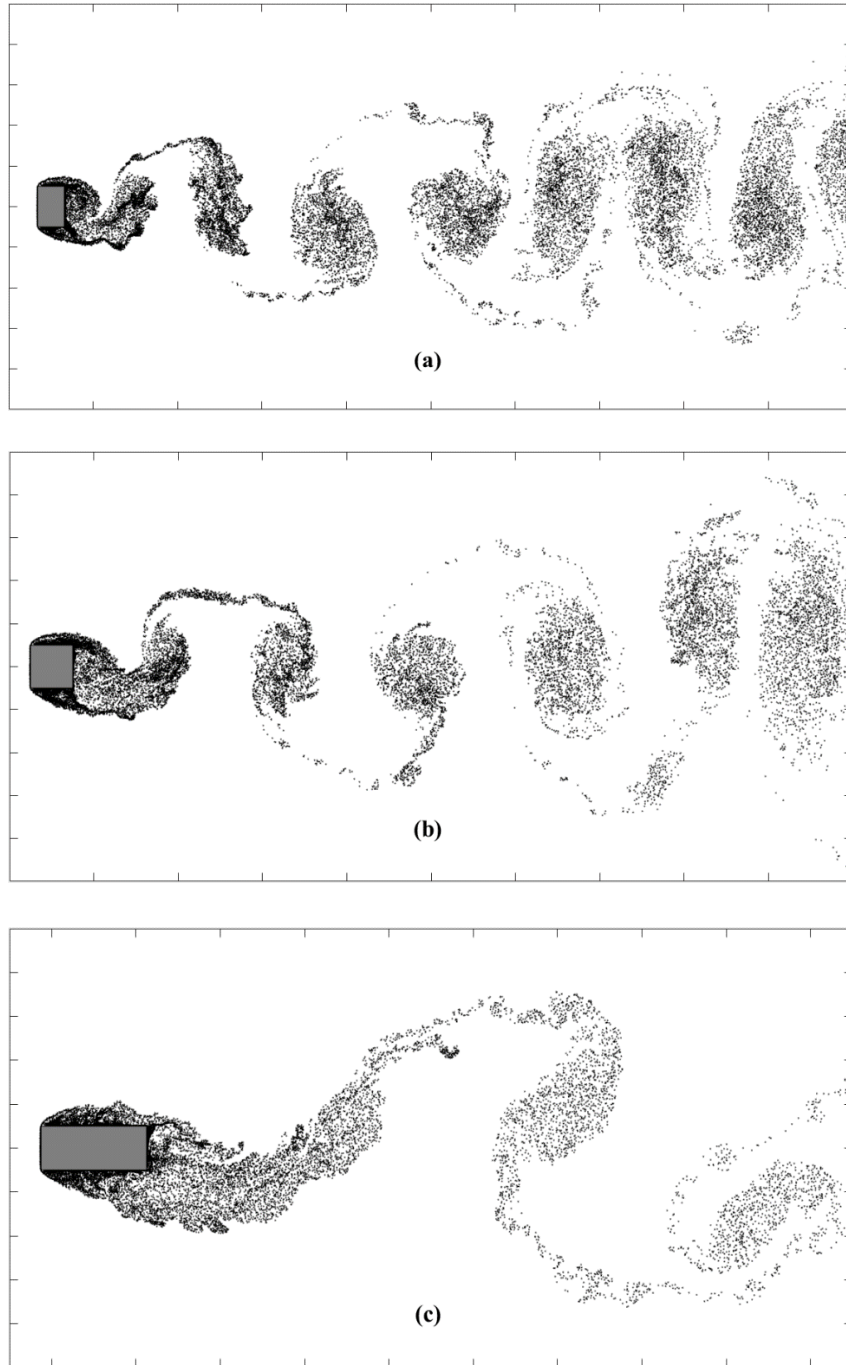
Figure 3-10. Distribution of vortices (a) B/D = 0.63 at t* = 90 (b) B/D = 1.0 at t* =94 (c) B/D=2.5 at t*=122

3.3. Flow Over Square Cylinder with Sharp and Chamfered Corners

As discussed before flow over bluff bodies with sharp edges like rectangular sections undergoes separation at corners, and forms vortices which shed from alternating edges periodically. In this section, DVM algorithm is validated by comparing the results of the experimental study conducted by Tamura (1999) on the flow over square section with sharp and chamfered corners.

In the present simulation free stream velocity is 18m/s, and the flow is uniform with Re of 30.000. The DVM simulations are performed with square cylinders having 1m side length and square section is used in two different geometrical forms which are sharp and chamfered corners. The breadth distance of the chamfered square section is 1/6 of the side length. The square cylinders with sharp and chamfered corner are hereafter denoted by S and C, respectively.
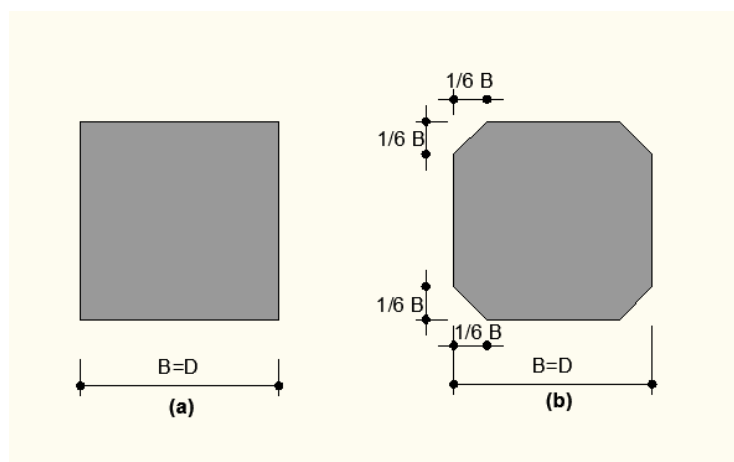
Figure 3-11. Square section with sharp (a) and chamfered (b) corners

Aerodynamic properties obtained from DVM solution and experimental results are presented in Table 3-3. It can be seen that DVM solution compare very well with experiments for predicted mean drag coefficient and root mean square of lift coefficient. It is notable that according to the experimental results, drag coefficient is reduced by %36 with corner cutting and 30% reduction is obtained from the DVM

simulation. Similarly, root mean square of lift coefficient is significantly reduced by 64 % experimentally and 44% is found in the present simulations. The change in the mean drag and rms of lift coefficient time series between two shapes are presented in Figure 3-12 and Figure 3-13, respectively.

Table 3-3. *Comparison of aerodynamic properties of DVM solution of flow over square section with sharp and chamfered corners*

Study	Section	C_{Davg}	C_{Lrms}	St
Tamura & Miyagi (1999)	S	2.10	1.10	0.13
DVM (Present)	S	2.15	1.06	0.14
Tamura & Miyagi (1999)	C	1.35	0.40	0.16
DVM (Present)	C	1.50	0.60	0.17
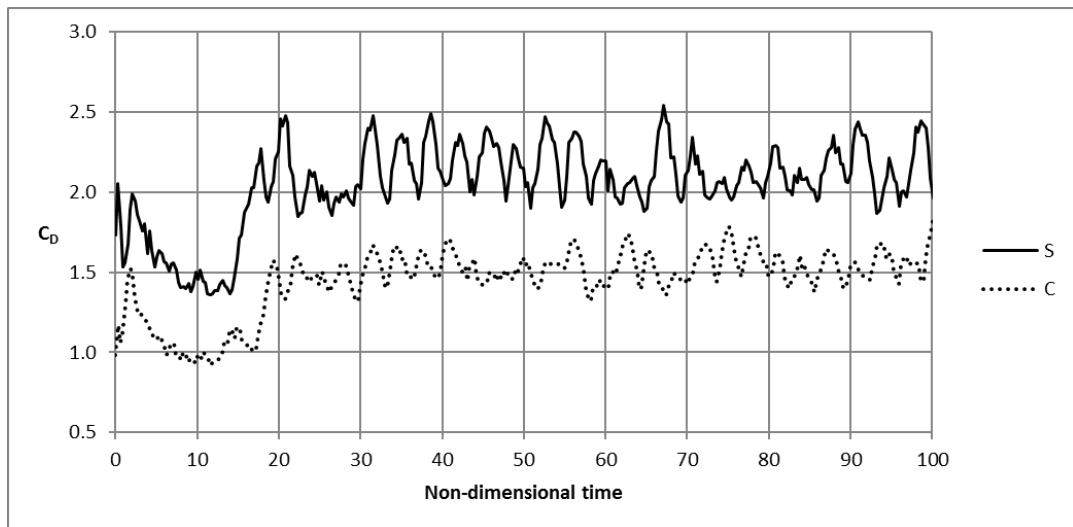
Figure 3-12. Drag coefficient of flow over square prism with sharp and chamfered corners
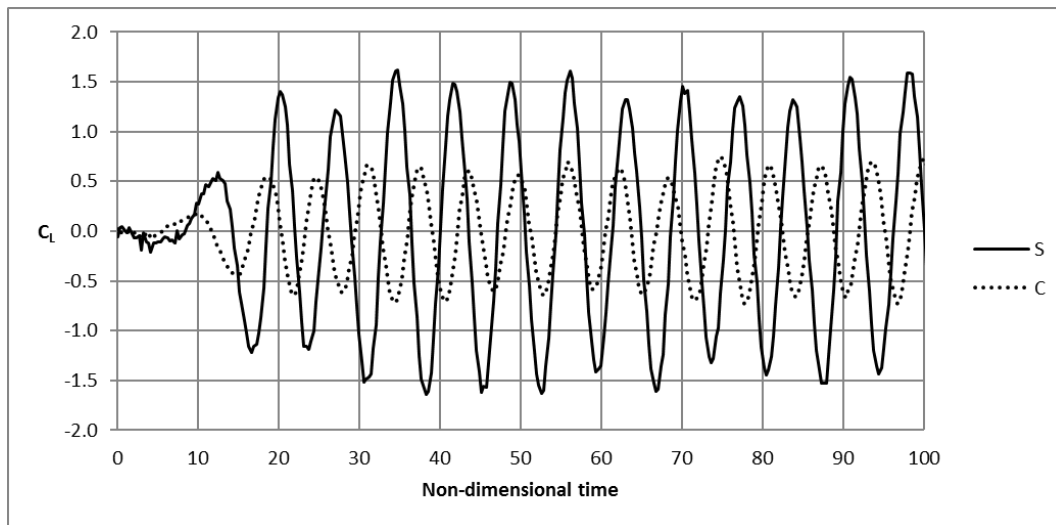
Figure 3-13. Lift coefficient of flow over square prism with sharp and chamfered corners

Despite to slightly overestimation for both cases, DVM shows that 18% of increment in Strouhal Number with corner cutting that is very close to the experimental value of 19%. Therefore, it can be concluded that the effect of corner shape is well simulated with DVM algorithm. In order to visualize flow field obtained from DVM solution for both shapes, distribution of vortices at an instant time is presented in Figure 3-14.
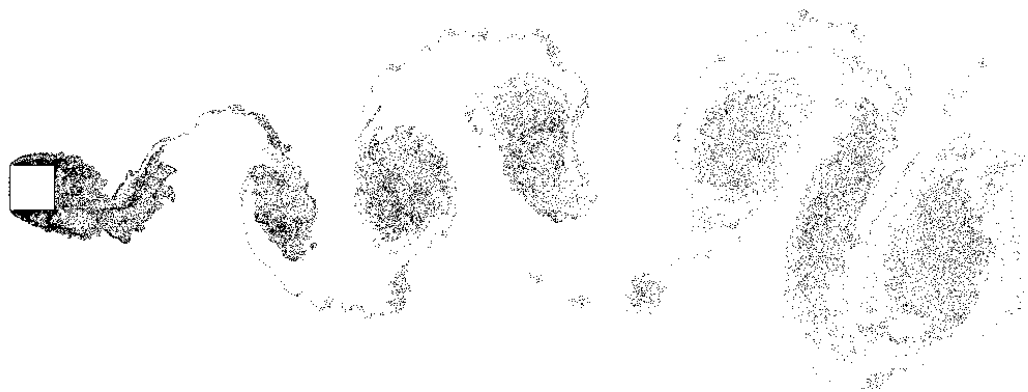
(a)

(b)

Figure 3-14. Flow at non-dimensional time 200 for RE=30.000 (a) S (b) C

3.4. Flow Over A Bridge Deck Section

Since long span suspension bridges are flexible and sensitive to wind loadings, aerodynamic aspects of the bridge deck sections have been attracted researcher's attention for several decades. Many experimental and numerical investigations have been concentrated on aerodynamic response of static and motion-free bridge deck sections with varying shapes.

DVM algorithm is validated with experimental results on the flow around rectangular sections so far and finally, due to aforementioned importance in the field of structural engineering, numerical algorithm is examined on the flow over a static bridge deck section. The mid span deck section of Great Belt East Bridge located in Denmark is selected for validation of DVM algorithm, since it has been extensively studied in numerous experimental and numerical analyzes.
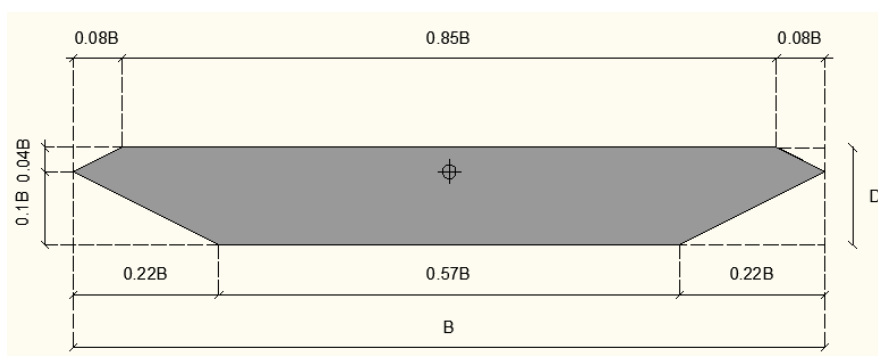
Figure 3-15. Dimension of the model section

The length scaled dimensions and notation of the model section are illustrated in Figure 3-15. In the present DVM simulation, free stream velocity is 20m/s corresponding Re of 19600. The calculations are performed at non-dimensional time step of 0.14 and the body is represented by 400 panels with equal size.

Results obtained from DVM are compared with other experimental and numerical investigations and presented in Table 3-4. Experimental studies compromised on St Number of 0.15. By making Fast Fourier Transform (FFT) analysis on the drag force signal, the dominant vortex shedding frequency is found to be 5.59 Hz with corresponding St of 0.16 which agrees with experimental value.

Table 3-4. *Comparison of aerodynamic properties of DVM solution of flow over the bridge deck section*

Study	C_{Davg}	C_{Lavg}	C_{Mavg}	St
DMI and SINTEF (1993) Exp	0.54	0.01	0.028	0.15
Terrés-Nícoli & Kopp (2009) Exp	-	0.08 – 0.10	-	0.15
Jenssen and Kvelmsdal (1999) FV	0.45	0.04	-	0.16
Larsen & Walther (1998) DVM	0.57	-	-	0.17
Morgenthal & Mcrobie (2002) DVM	0.42	0.08	-	0.19
Present DVM	0.50	0.12	0.022	0.16
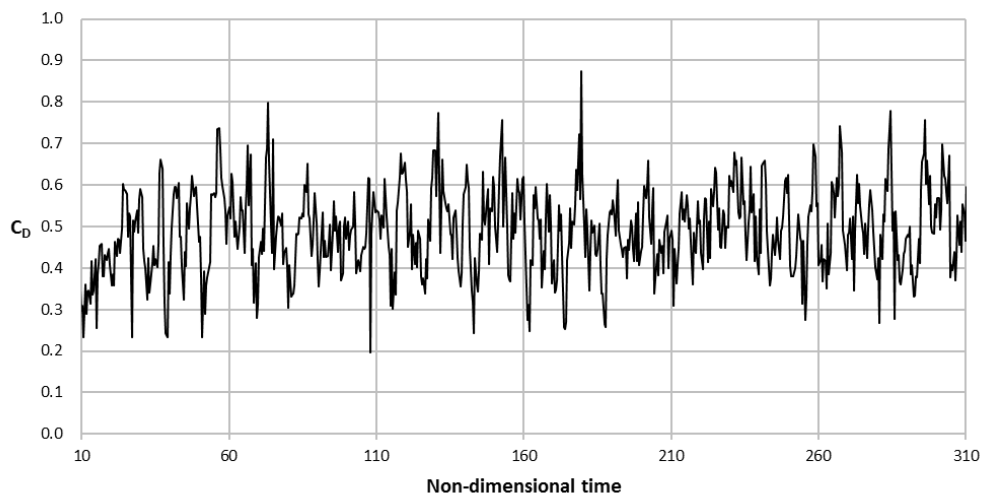
Figure 3-16. Drag coefficient time series obtained from DVM for flow over the bridge deck section
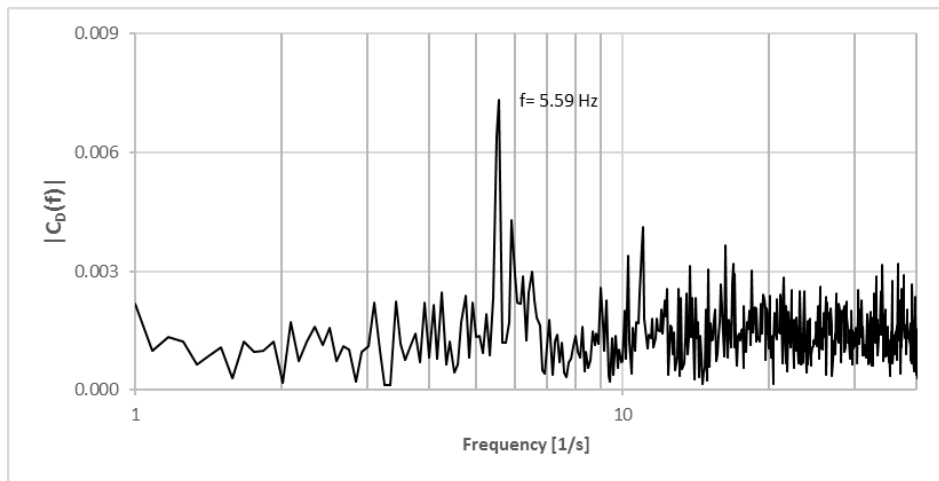
Figure 3-17. Spectrum of drag coefficient for flow over the bridge deck section

The predicted mean lift coefficients from different experimental and numerical studies are in the range of $0.01 - 0.10$ close to 0. It is overestimated with value of 0.12 in the present DVM simulation. Similar to the results obtained from DVM simulations on rectangular sections which are previously discussed, DVM algorithm used tends to overestimate lift forces, and it is attributed to relatively poor prediction of pressure distribution over the top and bottom surface. For the bluff bodies having higher aspect ratio (B/D), reattachment of shear layer may occur on the streamwise surfaces and therefore numerical methods have a tough challenge with predicting approximate reattachment point towards the trailing edges. Mean pressure distribution from DVM solution and an experiment are illustrated in Figure 3-18 and Figure 3-19 respectively.
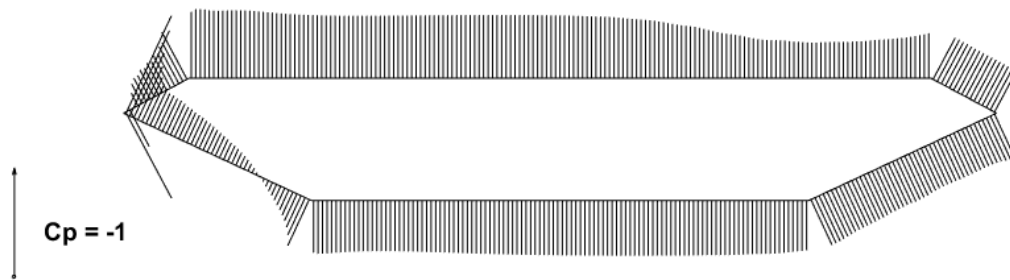
Figure 3-18. Distribution of average pressure coefficient (C$_P$) for different non-dimensional time step size (Δt*)
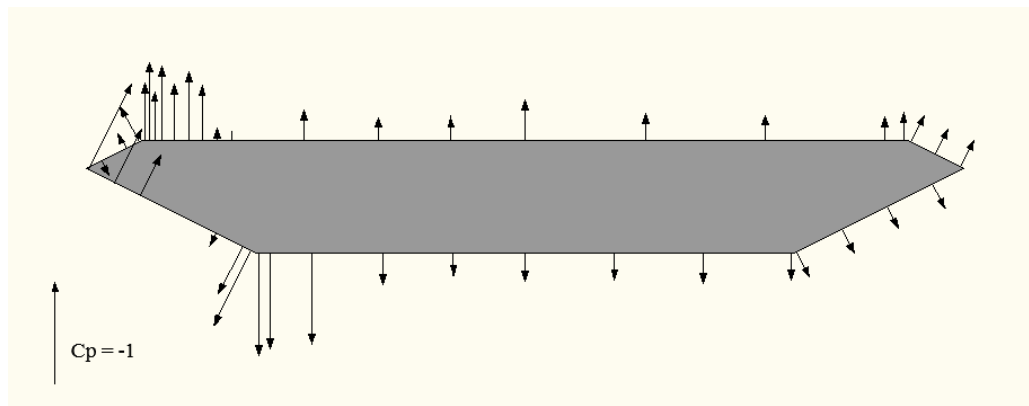
Figure 3-19. Average pressure distribution obtained from wind tunnel experiment with 1:70 scaled section model conducted by Terrés-Nícoli & Kopp *(2009)*

In general, mean pressure distribution from DVM compares well with the experiment, though local peak suction on the leading edges of the top and bottom surface are not captured. The reasonable explanation of this discrepancy is that the streamwise length of the recirculation zone may be overestimated on both surfaces which shift the pressure recovery towards trailing edge on upper surface. To illustrate situation, instantaneous flow pattern and vortex particle distribution are illustrated in Figure 3-20. It can be seen that reattachment of flow occurs beyond midpoint of the top surface, and shear layer extends to downstream edge of the bottom surface.
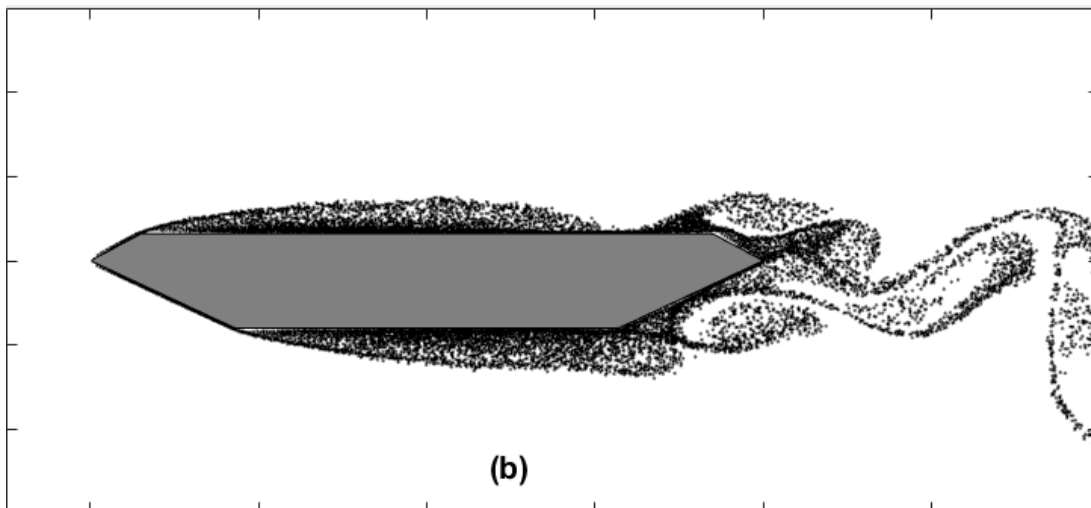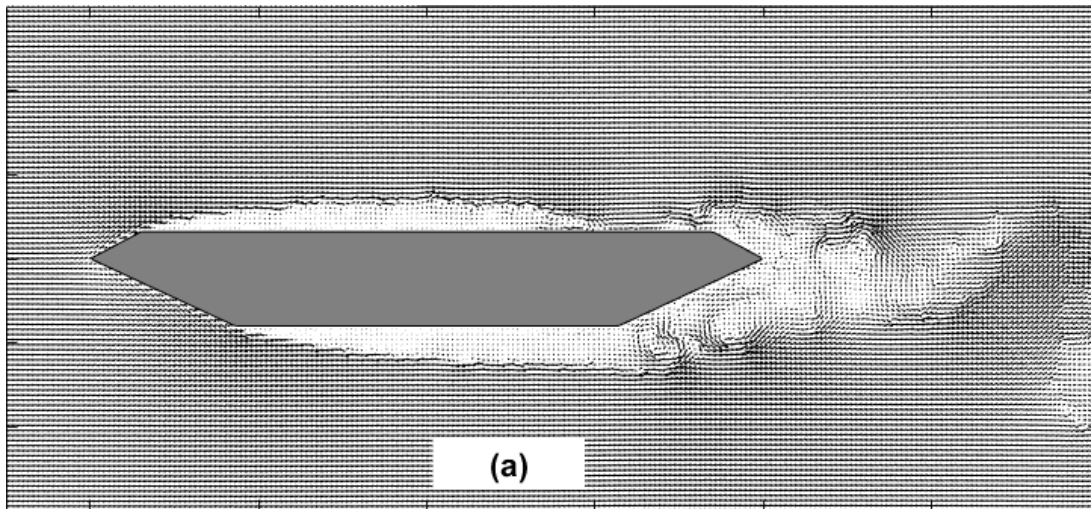
Figure 3-20. Flow at non-dimensional time 174 for Re = 24500

CHAPTER 4

PARAMETRIC STUDY

In a vortex cloud, discrete vortices are characterized by their strength and position on the simulation domain. The solution of flow properties with DVM algorithm is very sensitive to the parameters used and therefore selection of the input parameters requires special treatment. Based on DVM applications with various parametric configurations on the flow past rectangular and bridge deck sections, the most important parameters are determined as time step size, panel size and grid size of convection calculations which highly affect consistency and numerical stability of the DVM solutions. In order to make advantage of DVM algorithm in terms of its ability of fast iterations and relative accuracy compared to the other complex numerical techniques, those model parameters should be selected optimally.

In this section effect of time step size, panel size and grid size on accuracy and numerical stability of the DVM calculations are investigated. While selecting one of them as a control parameter, other input parameters are kept constant. At the first stage, parametric study is carried out on the DVM solution of flow over the square section due to its simplicity and wide usage in many structural engineering applications. The same procedure has been followed on the DVM calculations on the flow over the mid-span deck section of Great Belt Suspension Bridge (Denmark). Influence of the control parameters on the solution is analyzed in terms of aerodynamic forces, pressure distribution and Strouhal number as a measure of vortex shedding frequency.

4.1. Parametric Study of Flow Past Square Prism

Parametric study is conducted for flow over static square section with zero angle of incidence to flow direction. Free stream velocity is 10 m/s with corresponding Re of

21800. Effect of time step size, panel size and grid size are analyzed in terms of aerodynamic forces and pressure distribution acting on the square section. Vortex shedding frequency is obtained by performing Fast Fourier Transform (FFT) on the force signal, and corresponding St is presented for each case.

4.1.1. Effect of Time Step Size

In the present study, non-dimensional time step is selected as the control parameter. 200 source panels with equal size are used and panel size Δs is correlated with vortex shedding distance (ε) and vortex core radius (d) such that: $\varepsilon=\Delta s/2$, $d=\Delta s/4$ as found to be satisfactory set of parameters for viscous flows by Spalart (1981) in his study. For convection calculations, grid system is used and grid size is selected as 0.05D in all directions.

At the first attempt, non-dimensional time step size was set to be 0.001 and after 50-time steps, the model became numerically unstable. The difference between consecutive value of lift and drag forces were excessively high. For the next simulations, time step size was increased until reasonable time series of force coefficients and formation of wake flow (existence of Karman Vortex Street) were achieved. After several attempts, it was concluded that solution of DVM on the flow model is not reasonable and numerically stable for the non-dimensional time steps lower than 0.01. Therefore, the effect of non-dimensional time step size is examined for the range of 0.01 - 0.2 in this study.

It is noted that the flow does not follow a regular oscillatory pattern for DVM with Δt^* lower than 0.08. The time histories of lift and drag force coefficients for $\Delta t^*=0.01$ between non-dimensional time 5 and 30 are shown in Figure 4-1 and Figure 4-2. At first glance, the oscillation does not seem to be fully developed however the general picture does not change after non-dimensional time of 30. Since square section is immersed to the free stream without angle of incidence, vortex shedding from far end corners is expected to be periodic. From the spectral analysis of lift force, the dominant frequency is found to be 0.53Hz corresponding to St of 0.066 (Figure 4-6-a) and does

42

not agree with experimental values given in Table 4-1. It is seen that increasing time step size tends to minimize the irregular lift coefficient time series and it reduces the noise level on the force signals. For $\Delta t^*=0.04$, there still exists irregularity in lift and drag coefficients even if it is not as much as for $\Delta t^*=0.01$. The most notable one can be seen approximately between non-dimensional time of 35 and 45 (see Figure 4-4 and Figure 4-5).
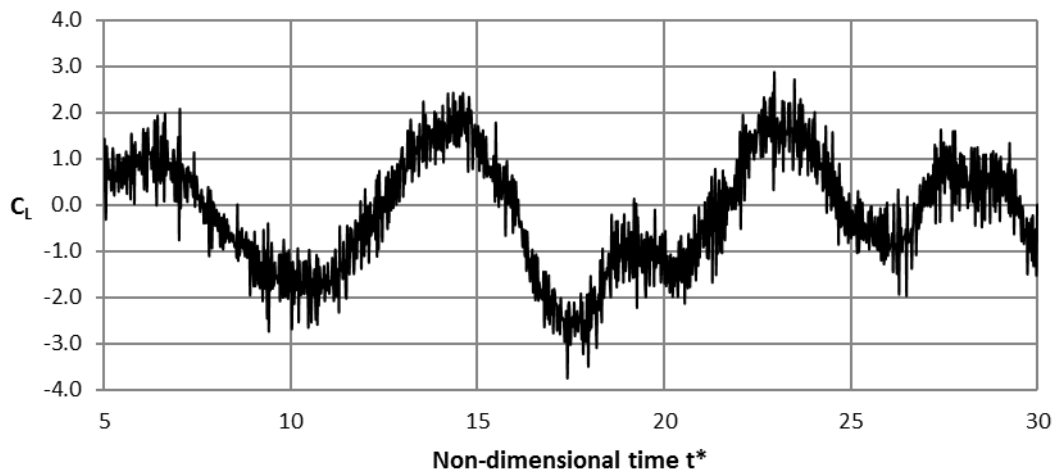

Figure 4-1. Coefficient of lift force for non-dimensional time step $\Delta t^*=0.01$
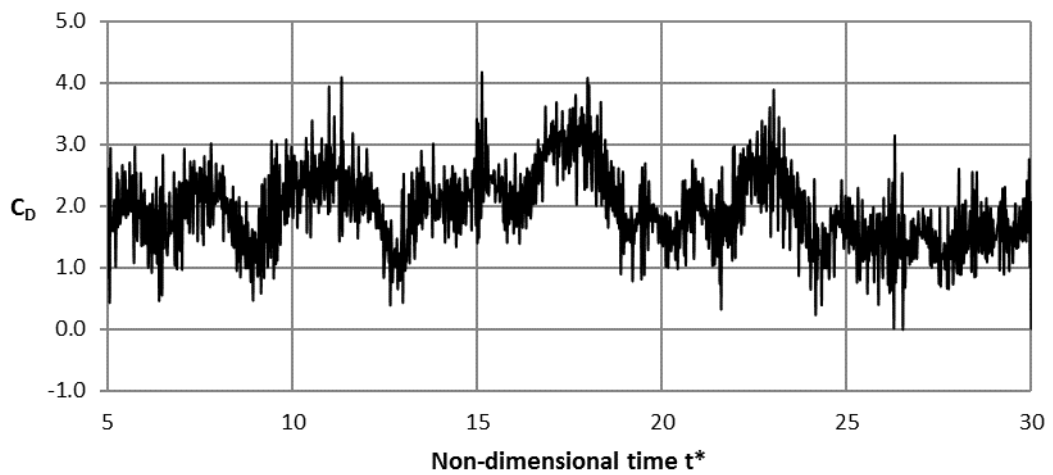
Figure 4-2. Coefficient of drag force for non-dimensional time step $\Delta t^*=0.01$

Considering lower time step size introduces more irregularity and noise level on the time history of the force coefficients, this can be attributed to significance of diffusive

displacement over convective displacement of vortex particles. Assuming that the velocity of a vortex particle does not change in two consecutive time steps, the convective displacement will be product of velocity and time step size. Therefore, convective displacement will be proportional to Δt. On the other hand, the average diffusive displacement of the particle will be proportional to $\sqrt{\Delta t}$ referring to random walk algorithm used. In the case of smaller time step size, convective and diffusive displacements are not decreased by the same ratio and significance of diffusive displacement will be higher. Besides, due to probabilistic nature of random walk method, the solution becomes noisier.

Table 4-1. *Comparison of aerodynamic properties of DVM solution of flow over the square section for different Δt^**

Study	Re	C_{Davg}	$C_L{}'$	St
Lee (1974) Exp	1.76e+5	2.07	1.23	0.12
Norberg (1993) Exp	1.3e+4	2.15	-	0.13
Vickery (1966) Exp	4.0e+4 - 1.6e+5	2.03	1.32	0.12
Taylar & Vezza (1999) DVM	2.0e+4	2.38	-	0.13
DVM (Δt^*=0.01)	2.18e+4	1.84	1.30	0.07
DVM (Δt^*=0.02)	2.18e+4	2.03	1.33	0.09
DVM (Δt^*=0.04)	2.18e+4	2.26	1.31	0.12
DVM (Δt^*=0.08)	2.18e+4	2.23	1.20	0.15
DVM (Δt^*=0.10)	2.18e+4	2.13	1.12	0.14
DVM (Δt^*=0.12)	2.18e+4	1.97	0.99	0.13
DVM (Δt^*=0.16)	2.18e+4	1.64	0.52	0.12
DVM (Δt^*=0.20)	2.18e+4	1.58	0.41	0.12

Initially average drag coefficient increases for increasing time step up to Δt^*= 0.08, at the same time RMS of lift fluctuation slightly decreases. When Δt^* is greater than 0.08, drag coefficient decreases, besides a notable drop is seen for Δt^*=0.16 in both C_{Davg}

and RMS of lift force fluctuation. Although DVM gives consistent value of St with experimental values for Δt^* greater than 0.12, they show poor performance on the prediction of aerodynamic force and pressure distribution.

(a)

(b)
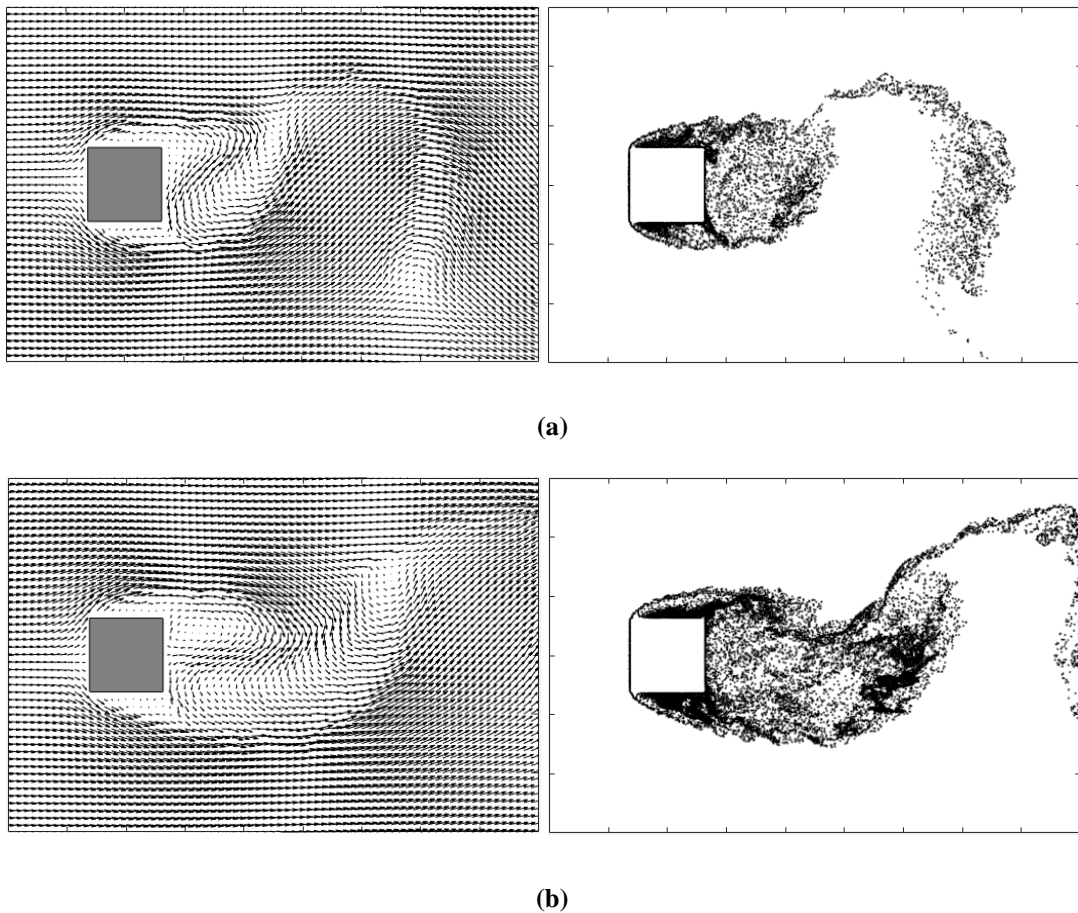
Figure 4-3. Visualization of vortex shedding (a) DVM (Δt^*=0.10) at t*=73.2 (b) DVM (Δt^*=0.16) at t*=85.44

The interesting feature noted is that increasing time step with respect to Δt^*=0.08 results in further stretched vortex structure formed at leeward corners along the wake stream. As an example, distribution of vortex particles (right) and vector illustration of velocity field (left) for Δt^*=0.10 and Δt^*=0.16 are shown in Figure 4-3 (a) and (b) respectively. Vortex formation from low leeward corner is captured for (a) at t^*=73.2

and for (b) at t^*=85.44 where the lift force reaches the maximum value in a cycle for both cases. Another related feature is observed on pressure distribution along the leeward face of the body. Figure 4-7 and Figure 4-8 show average pressure distribution and standard deviation distribution of fluctuating pressure on the square section obtained for different Δt^*. As it can be seen, the distribution of average pressure coefficient tends to increase (lower suction) and a notable difference is obtained for Δt^*=0.16. Since vortices shed from the far end corners and growing vortices are primary reason of the strong pressure fluctuation on the leeward face, stretching of vortices with increasing time step may decrease the suction. A similar finding has been showed by Bearman and Trueman (1972) that higher distance of leeward side to the vortices formed, the less suction there will be.
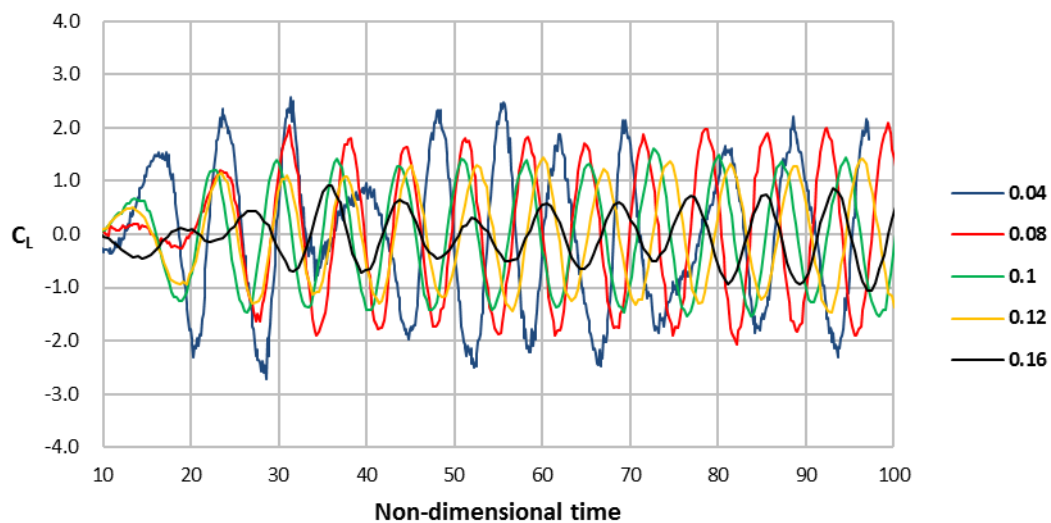
Figure 4-4. Lift coefficient (C_L) for different Δt^*
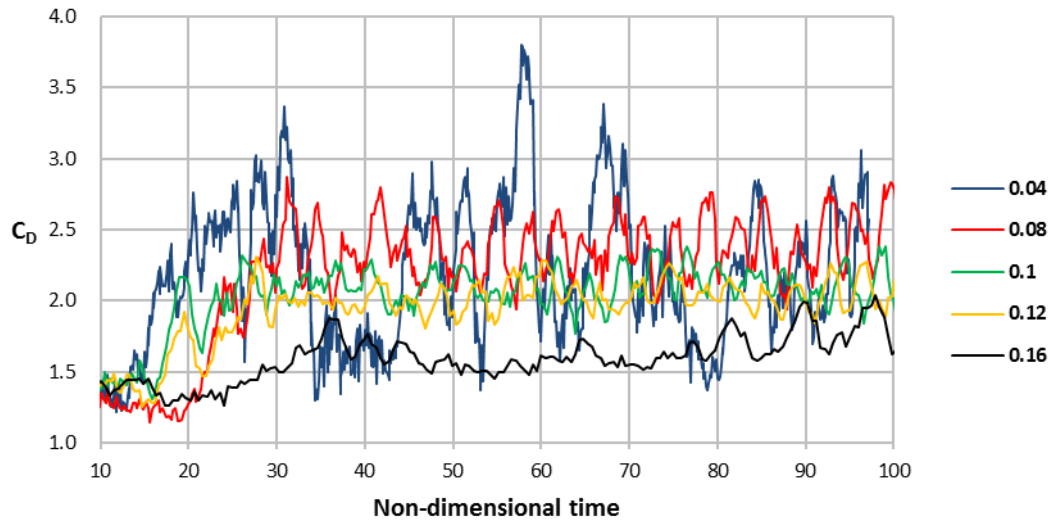
Figure 4-5. Drag coefficient (C$_D$) for different Δt^*
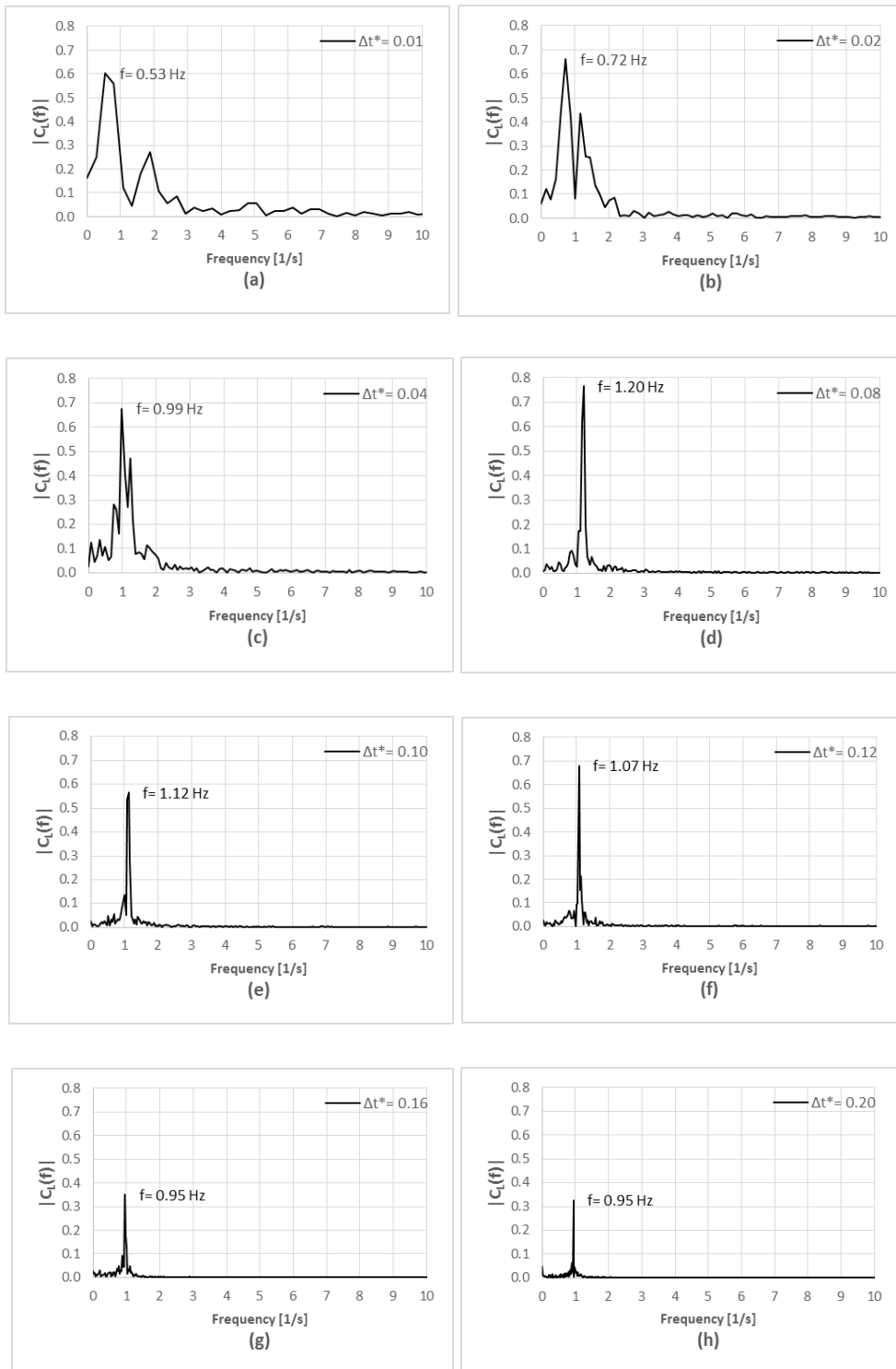
Figure 4-6. Spectra of lift coefficients (C$_L$) corresponding to Δt*

For the face A-B, all DVM simulations except for $\Delta t^*=0.01$ are almost identical and compare well with experiments in terms of average pressure distribution. The DVM simulations with $\Delta t^*=0.16$ and $\Delta t^*=0.20$ perform poorly for other faces in terms of average pressure distribution. Another important inference from the Figure 4-7 is that distribution of C_{Pavg} along the faces BC, CD and AD is asymmetric for Δt^* smaller than 0.08. It is attributed to statistical noise due to high penetration of random walk displacements for small time steps as discussed earlier. Another symptom of this issue can be seen in Figure 4-8 that standard deviation of pressure coefficient increases with decreasing Δt^*.
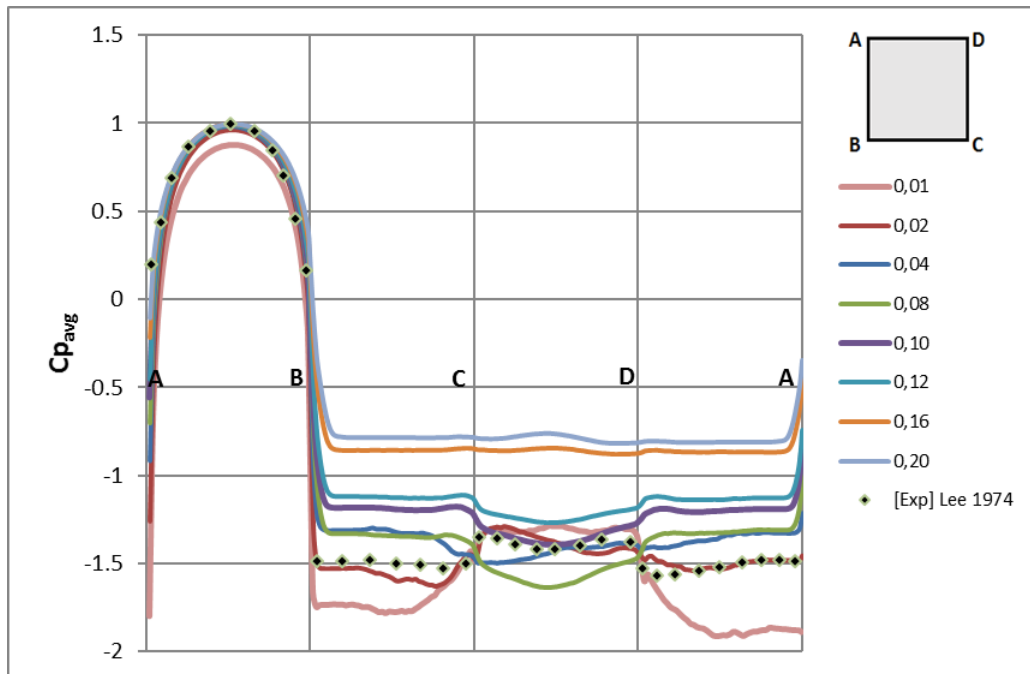
Figure 4-7. Distribution of average pressure coefficient (C_{Pavg}) for different Δt^*
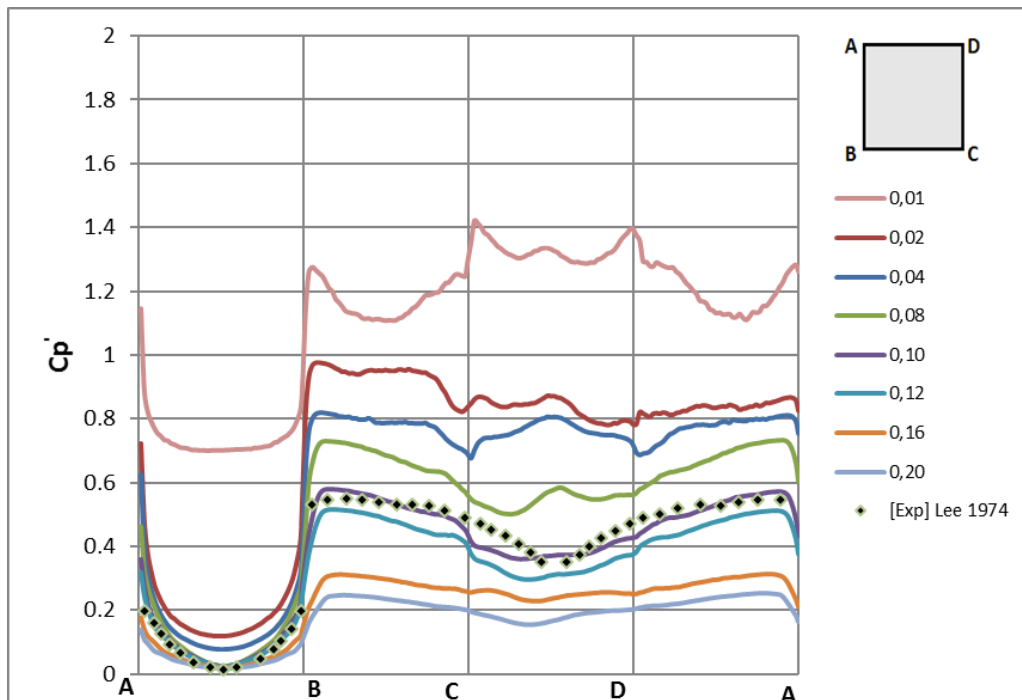
Figure 4-8. Distribution of standard deviation of fluctuating pressure coefficient (C_P') for different Δt^*

Results of the present DVM simulations showed that time step size defines the effectiveness of convection and diffusion process which in turn affects consistency of the flow solution. It is seen that smaller time step size amplifies diffusive displacements compared to convective displacements. In addition, solution becomes noisier due to probabilistic nature of random walk algorithm. It is also seen that convection of particles has stronger influence on the flow field than diffusion for increasing time step. In that case, vortices formed behind the body stretches along the flow direction that causes reduction in the suction on the leeward face.

4.1.2. Effect of Panel Size

The effect of panel size on DVM solution of flow over square prism is conducted. The number of panels is chosen as varying control parameter whereas other model inputs are kept as same. Since the only varying parameter is the panel number, the parameters ε and *d* are no more related to panel size, and set to be 0.0125m and 0.00625m, respectively as used in the section 4.1.1. According to the DVM results in section

4.1.1, the most consistent results are obtained for non-dimensional time step (Δt^*) between 0.08 and 0.12 and therefore in this study Δt^* is chosen to be 0.1 for all DVM simulations. Grid system is used in the convection calculation and size of the square grid is set to be 5% of the side length of square.

DVM model is initiated with number of 10 panels and increased up to 75 at the first stage. For all cases, the particles are seemed to be randomly distributed and no signs of shear layer on the side face and vortices at the wake were found. The reasonable flow pattern and aerodynamic forces are obtained by using 100 source panels, and surprisingly there is no transition of wake formation between 75 and 100 panels as it can be seen the distribution particles at $t^*=141.2$ in Figure 4-9. Therefore, it is concluded that the sufficient number of vortex particles is approximately 100 for $\Delta t^*=0.10$ in order to satisfy reasonable flow pattern. The effect of panel size on DVM solutions are examined between number of 100 and 300 panels in this section.
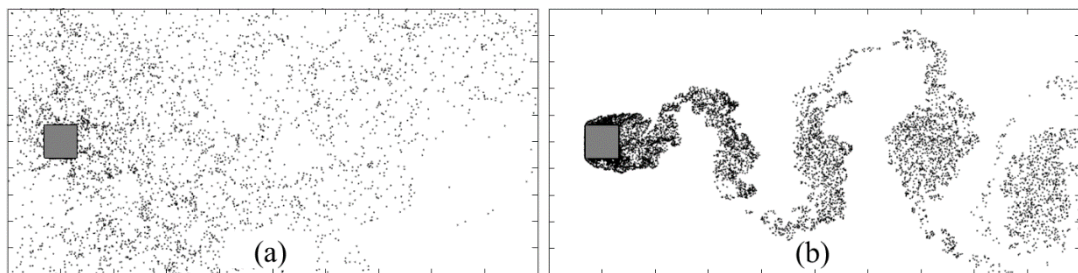
Figure 4-9. Distribution of particles at t*=141.2 with total panel numbers (a) 75 (b) 100
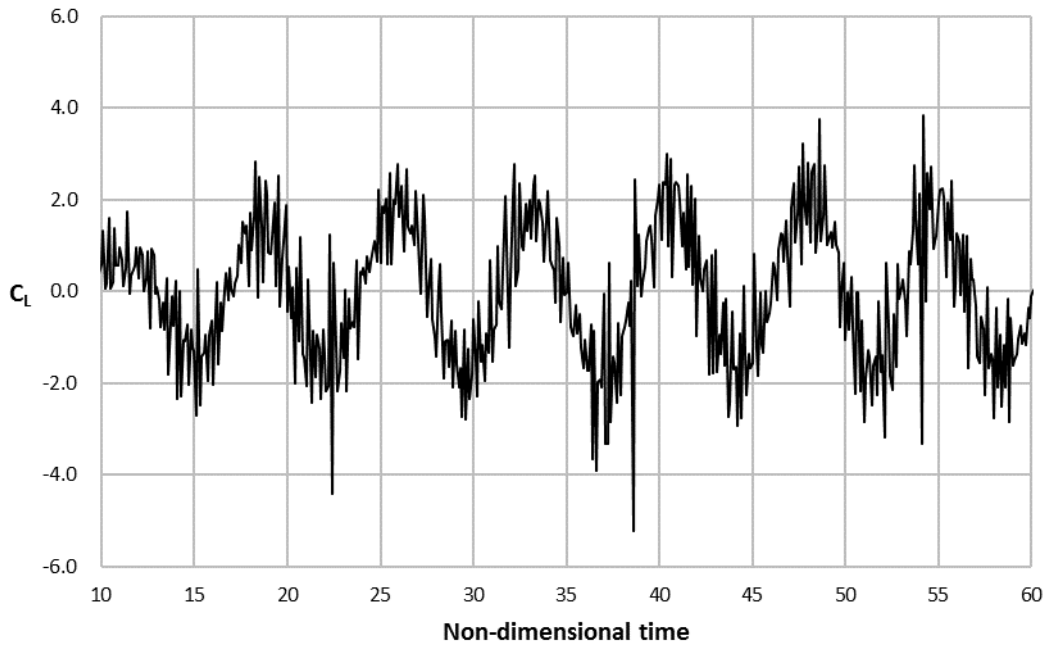
Figure 4-10. Coefficient of lift force for panel number 100
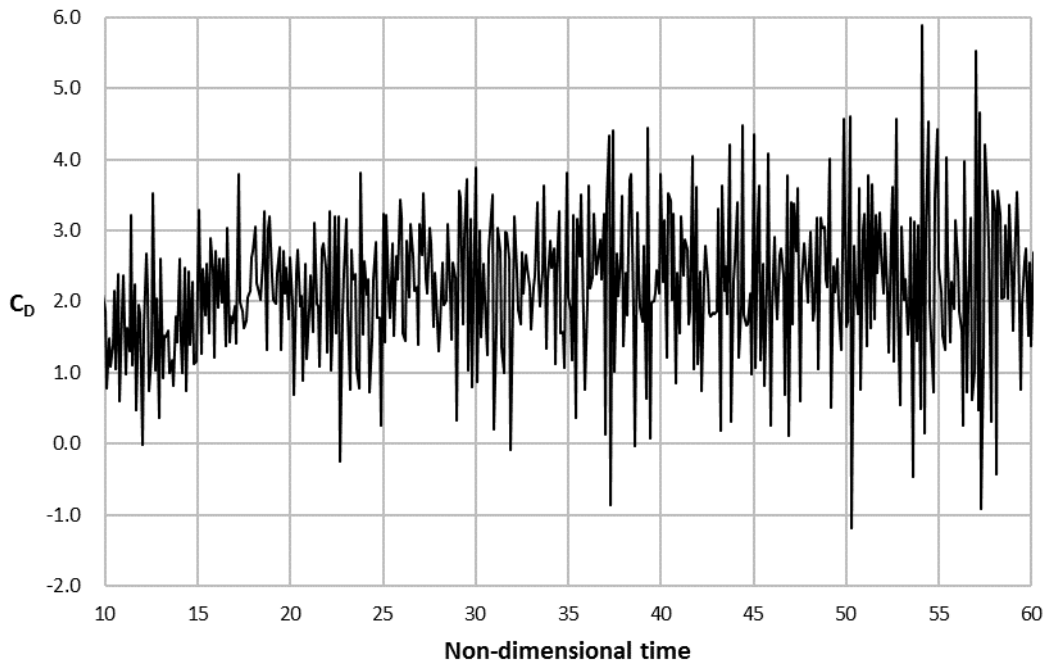
Figure 4-11. Coefficient of drag force for panel number 100

Figure 4-10 and Figure 4-11 show lift and drag force coefficient time history for DVM simulation with total number of 100 panels respectively. A regular oscillatory pattern is achieved in the lift time series, but numerical noise is so excessive that there exists negative value of drag coefficient time series given in Figure 4-11. It may be also the symptom of overestimation of St (see Table 4-2). Although average pressure distribution is seen to be well captured for DVM solution with 100 source panels on the side faces BC and AD (Figure 4-12), it is expected to perform better for the face AB compared to other faces since complex wake formation and vortex shedding results in strong pressure fluctuation on the side and leeward faces. Therefore, there is no physical explanation of matching numerical and experimental results on the side faces but rather underestimation of pressure distribution in all faces results in close to experimental values along the face BC and AD by coincidence. All DVM simulation except that total number of 100 source panels give very similar results in terms of average pressure distribution on the body surface and results are in good agreement with the experiment (see Figure 4-12). On the other hand, panel number greater than 180 compare very well with experimental result in terms of standard deviation of pressure fluctuation on the surface.

Table 4-2. *Comparison of aerodynamic properties of DVM solution of flow over the square section*
for different panel numbers

Study	Re	C_{Davg}	C_L'	St
Lee (1974) Exp	1.76e+5	2.07	1.23	0.12
Norberg (1993) Exp	1.3e+4	2.15	-	0.13
Vickery (1966) Exp	4.0e+4 - 1.6e+5	2.03	1.32	0.12
Taylor & Vezza (1999) DVM	2.0e+4	2.38	-	0.13
DVM-100	2.18e+4	2.45	1.50	0.16
DVM-120	2.18e+4	2.21	1.17	0.15
DVM-160	2.18e+4	2.16	1.15	0.14
DVM-180	2.18e+4	2.16	1.14	0.14
DVM-200	2.18e+4	2.13	1.12	0.14
DVM-220	2.18e+4	2.11	1.09	0.14
DVM-240	2.18e+4	2.11	1.09	0.14
DVM-260	2.18e+4	2.10	1.08	0.14
DVM-300	2.18e+4	2.10	1.08	0.14
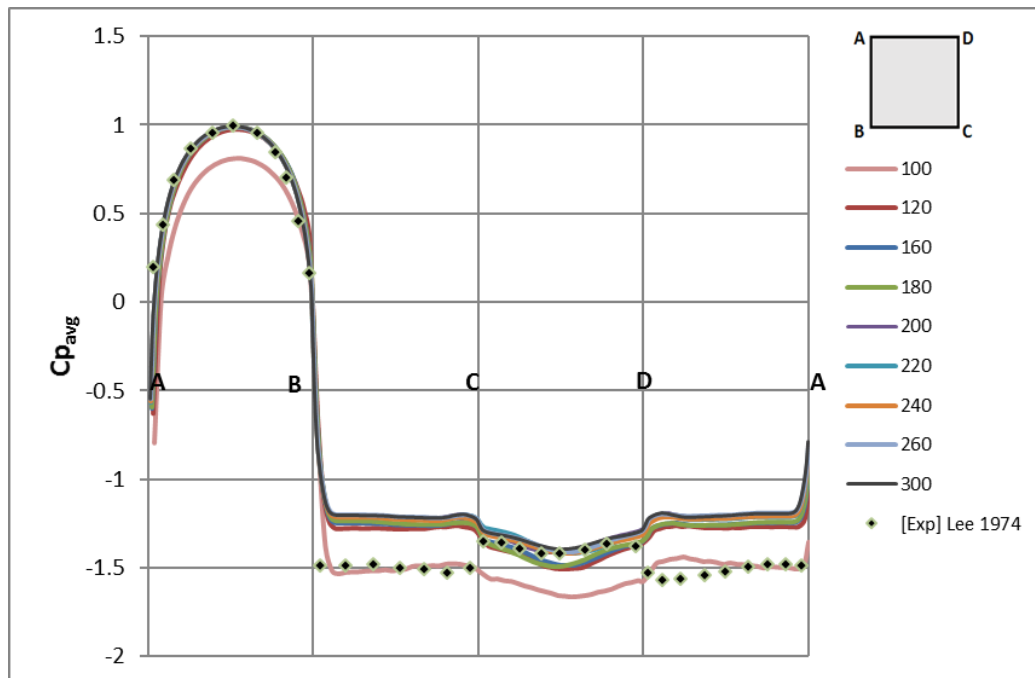
Figure 4-12. Distribution of average pressure coefficient (C_{Pavg}) for different panel numbers
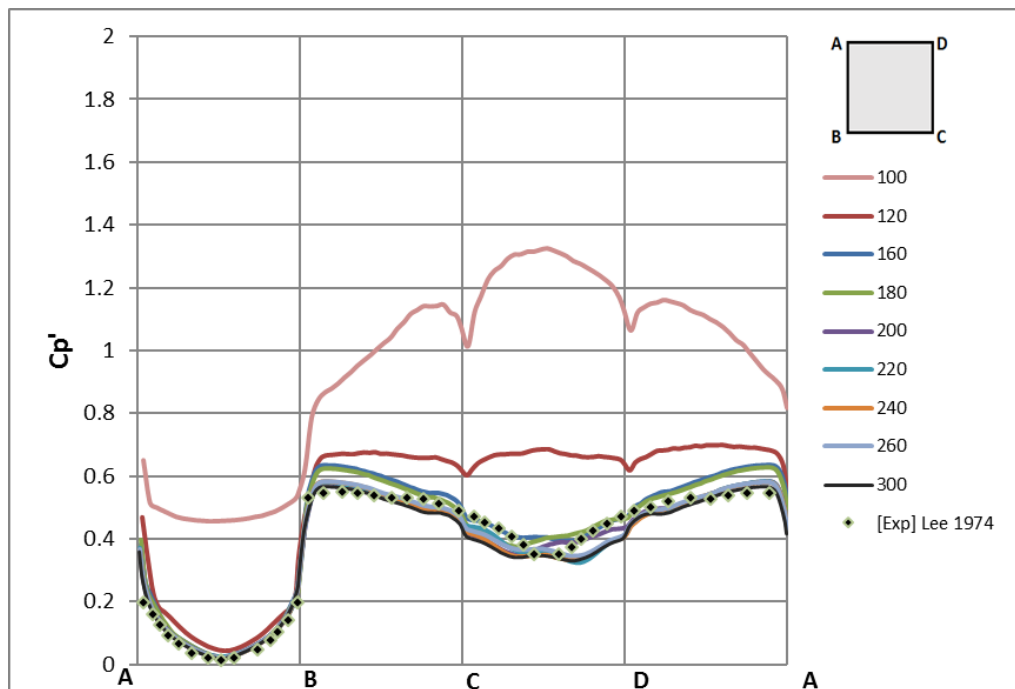
Figure 4-13. Distribution of standard deviation of fluctuating pressure coefficient (C_P') for different panel numbers

FFT analysis on the lift coefficient is performed for different number of panels used in the present DVM simulations and the spectra of lift coefficient signal are given in Figure 4-16. It is seen that the dominant frequencies of the lift fluctuation are very close to each other for DVM solution with panel numbers greater than 120. In fact, any significant variations of aerodynamic properties have been experienced for all DVM solutions except the one with 100 panel numbers. In addition, the flow solution tends to preserve its characteristics for further increasing panel numbers. The effect of increasing panel numbers is notably on reduction of noise level and it can provide better resolving of the near wake in return of computational expense. From the structural engineering point of view, prediction of the forces and pressure distribution, and their variations in time are the primary objective and it is concluded that 200 sources panels are sufficient to obtain consistent results for DVM simulation of flow over square prism with Re of 21800.
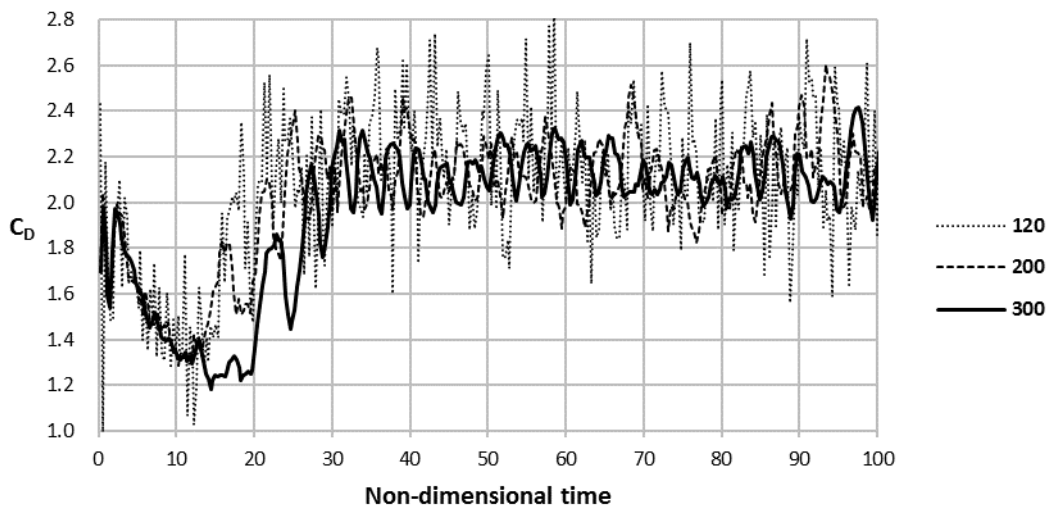
Figure 4-14. Drag coefficient (C_D) for panel numbers 120, 200 and 300
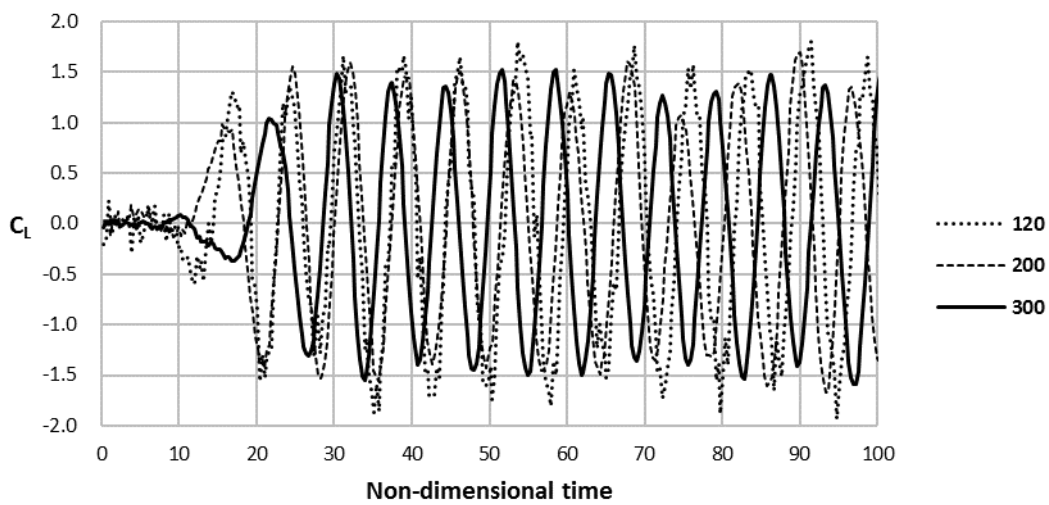
Figure 4-15. Lift coefficient (C_L) for panel numbers 120, 200 and 300

The most important feature noted in this section is that stability of the flow is not obtained until number of panels is increased to 100 and a reasonable flow pattern is

56

not seen for DVM with smaller panel numbers. This situation, in fact, supports the satisfactory sets of parameters recommended by Spalart (1981) for DVM with random walk method. Those length scale parameters act as important balance between diffusion and convection of particles especially around the vicinity of the wall. Shukla and Eldredge (2007) concerned about panel discretization in his study that high ratio of spacing between centers of two adjacent panels to vortex shedding distance from the wall may lead to domination of sheet diffusion over the vorticity transfer from each panel to neighboring particles which results in instability of the simulation.
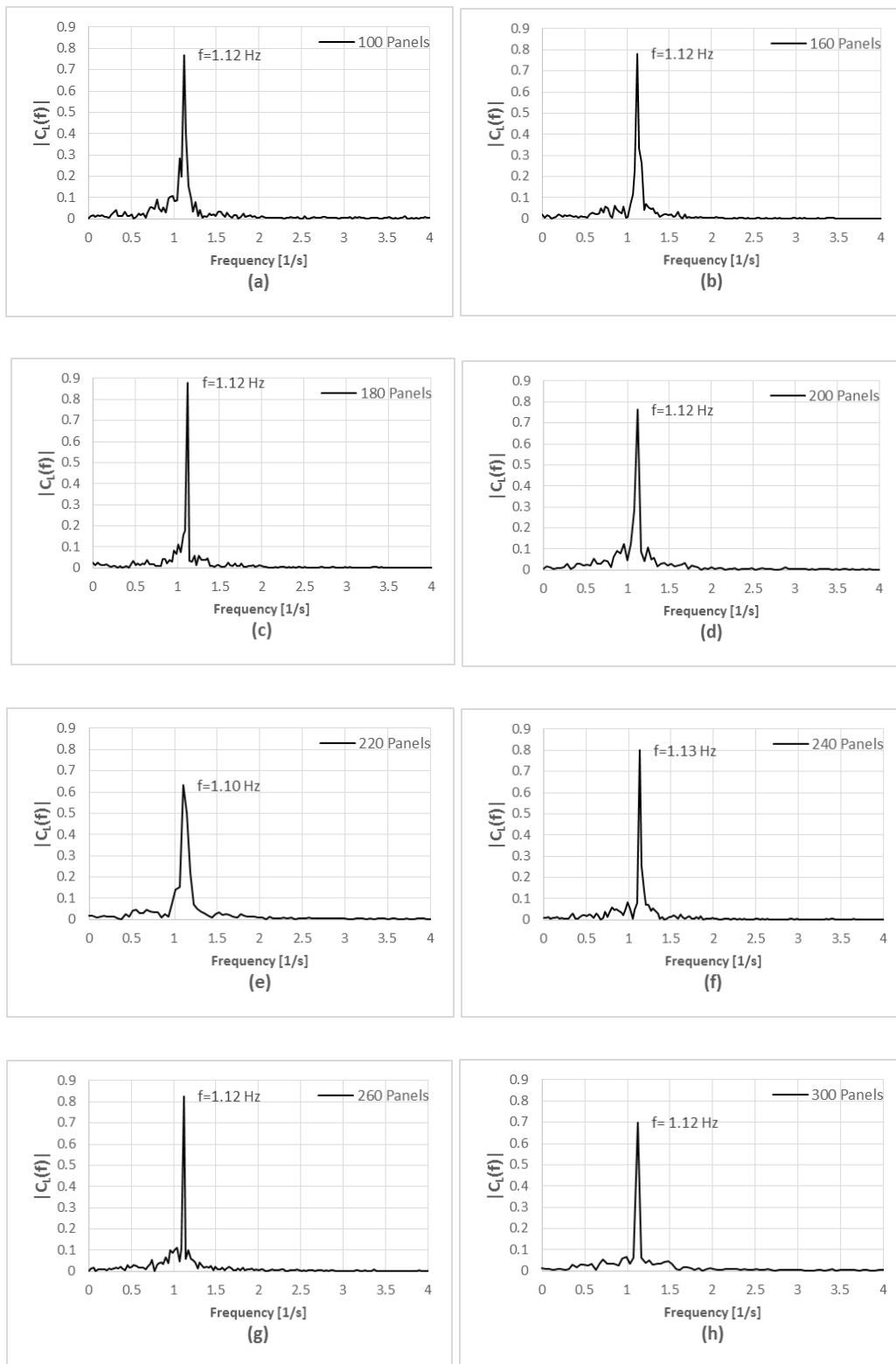
Figure 4-16. Spectra of lift coefficients (C$_L$) corresponding to number of panels used

4.1.3. Effect of Grid Size

In this section, effect of grid size on DVM solution of flow over square section is conducted. As discussed before, grid system defines the boundary of the solution domain. While changing the grid size, the domain size is kept constant for all simulations by adjusting the number of grids in each direction accordingly.

In the previous sections, effect of panel size and time step size are analyzed for flow over the square section. The most consistent results are obtained for the cases where Δt^* are within the range of 0.08 and 0.12. It is also seen that DVM simulations with total number of panels greater than 200 does not have any notable influences on the average forces and pressure distribution. In parallel with these findings, the present DVM simulations are carried out with $\Delta t^* = 0.1$ and 200 source panels. Panel size (Δs) is correlated with vortex shedding distance (ε) and vortex core radius (d) such that: $\varepsilon = \Delta s/2$, $d = \Delta s/4$.

Grid size is gradually decreased and increased with initial value of 0.05D as used in the previous sections and DVM solution without grid system is also carried out to find out whether use of grid system causes loss of accuracy or not. Considering the aerodynamic properties given in Table 4-3, DVM solution without grid system is well agreed with experimental results. On the other hand, a negligible loss in accuracy is seen when the model is initialized with grid system of 0.0125D cell size. Since decreasing grid size requires longer computation time, grid size of 0.0125D is selected to be lower limit of this section.

Table 4-3. *Comparison of aerodynamic properties of DVM solution of flow over the square section for different grid size*

Study	C_{Davg}	$C_L{'}$	St
Lee (1974) Exp	2.07	1.23	0.12
DVM (non-grid)	2.13	1.18	0.13
DVM (0.0125D)	2.18	1.16	0.14
DVM (0.025D)	2.13	1.14	0.14
DVM (0.04D)	2.11	1.12	0.14
DVM (0.05D)	2.13	1.12	0.14
DVM (0.10D)	2.05	0.94	0.15
DVM (0.20D)	1.89	0.70	0.14
DVM (0.40D)	1.46	0.45	0.15

Although the most consistent results compared to experimental is obtained with non-grid DVM solution in terms of force coefficients and Strouhal number, grid based DVM results indicates slightly loss in accuracy except of those with grid size larger than 0.10D (Table 4-3). By making FFT analysis on the lift force signals, the dominant frequencies are found to be between 1.09 and 1.17 Hz (Figure 4-18) and it is seen that vortex shedding frequency is not influenced considerably compared to force coefficients.
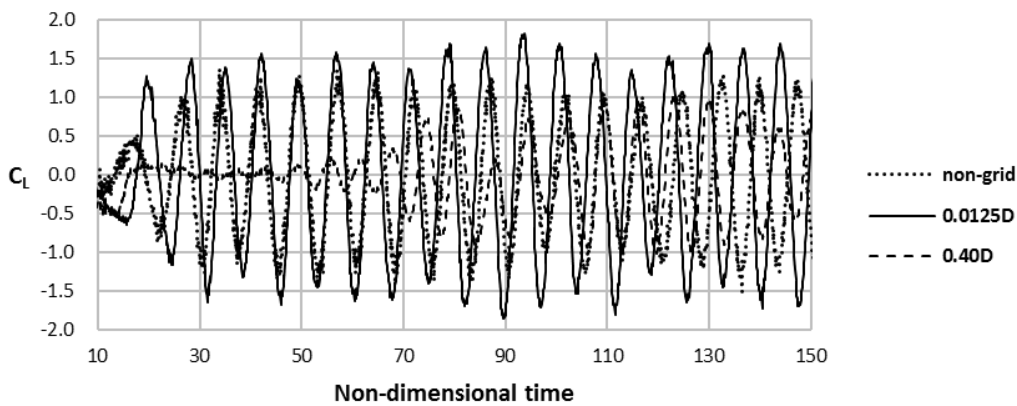
Figure 4-17. Coefficient of lift (C_L) with respect to non-dimensional time
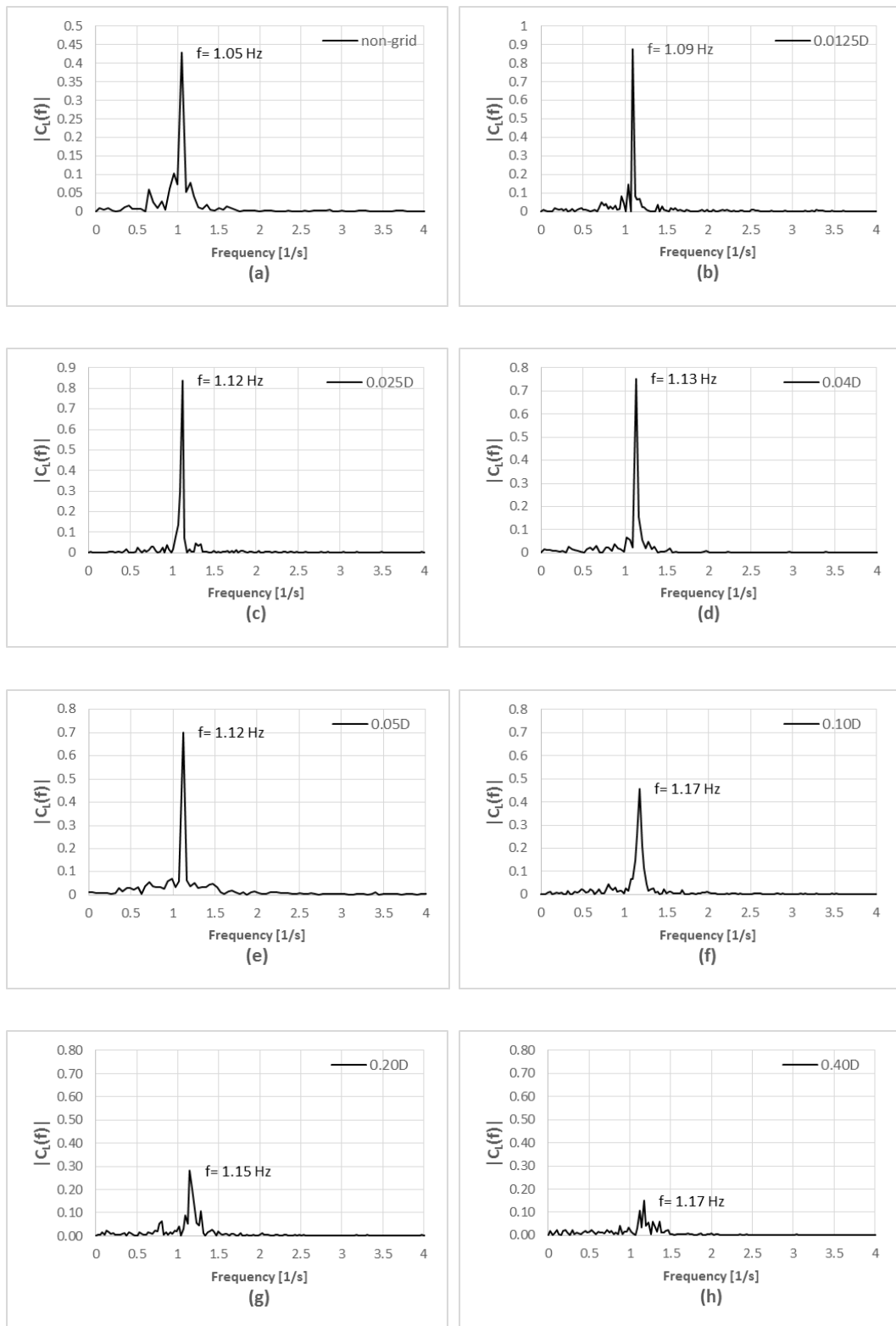
Figure 4-18. Spectra of lift coefficients (C$_L$) corresponding to grid size
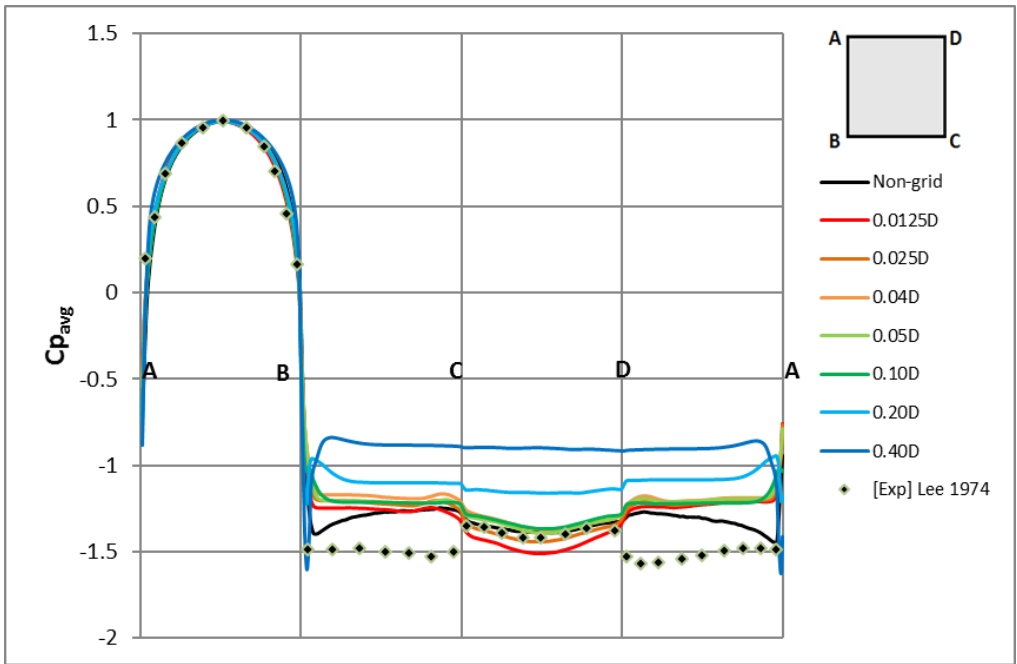
Figure 4-19. Distribution of average pressure coefficient (C_{Pavg}) for different grid size
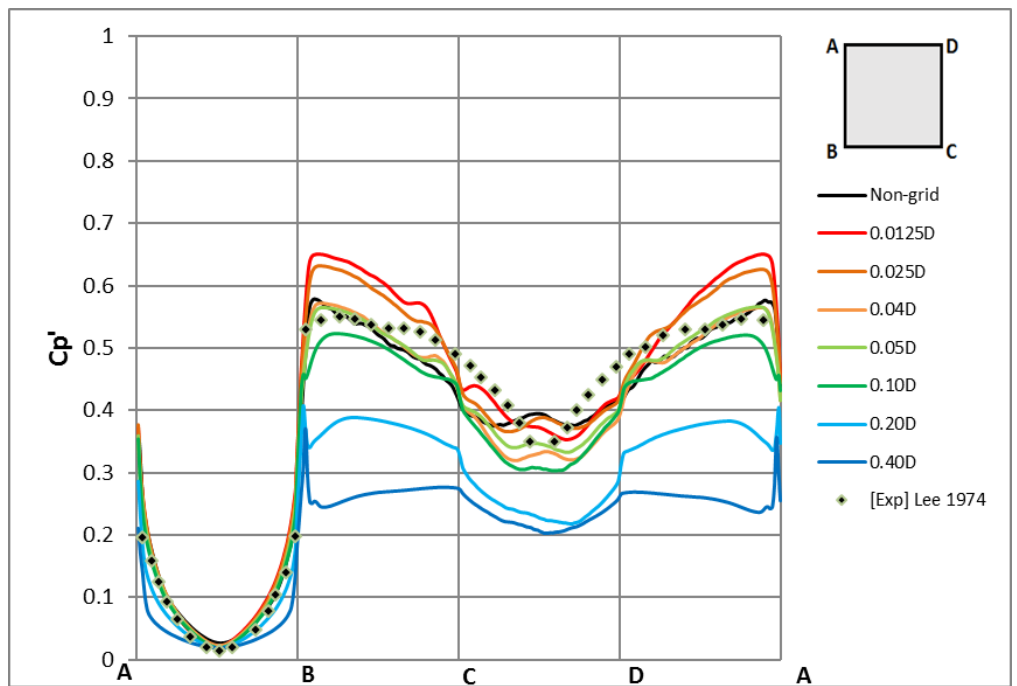
Figure 4-20. Distribution of standard deviation of fluctuating pressure coefficient (C_{P}') for different grid size

Mean and standard deviation of pressure distribution are given in Figure 4-19 and Figure 4-20, respectively. It is noted that DVM solution between grid size 0.0125D and 0.1D give similar results in terms of mean pressure distribution. On the other hand, standard deviation of pressure fluctuation on the side face is overestimated for grid size 0.0125D and 0.025D. In fact, the results of smaller grid size are expected to close to non-grid DVM solution by resolving fine scale flow field. Therefore, the reason of this discrepancy is not clear. A reasonable explanation was made by Taylor and Vezza (1999) in their study that 2D CFD models are not capable of representing 3D wake effects, i.e. streamwise component of vorticity due to vortex stretching.

4.2. Parametric Study on Flow Over Bridge Deck Section

In this section, parametric study is conducted for DVM simulations of flow over static bridge deck section with zero angle of incidence to flow direction. Free stream velocity is 20 m/s with corresponding Re of 19600.

Effect of time step size, panel size and grid size are analyzed in terms of aerodynamic forces and pressure distribution acting on the square section. Vortex shedding frequency is obtained by performing FFT on the drag force signal, and corresponding dominant frequency of the oscillation is presented for each case.
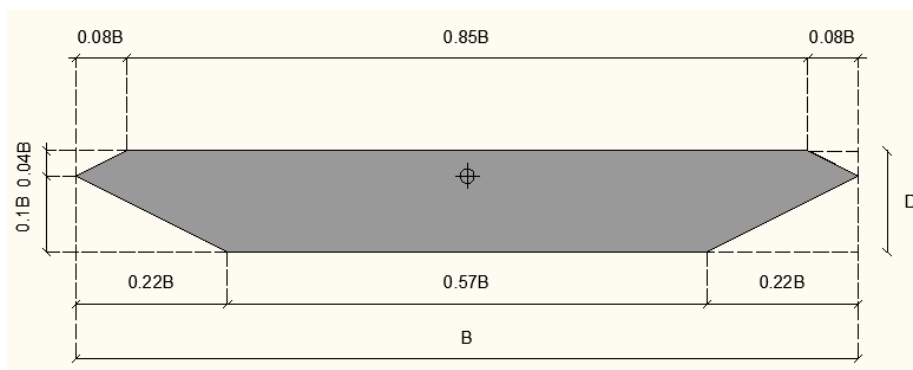
Figure 4-21. Length scale of the bridge deck section

4.2.1. Time Step Size

In the present study, non-dimensional time step is selected as the control parameter. 400 source panels with equal size are used and length scale parameters defined in the previous section are used. For convection calculations, grid system is used and grid size is selected as 0.05B in all directions. In order to be consistent with experiments, characteristic length (L) is selected as height (D) for drag coefficient calculations and width (B) for lift coefficient calculations referring to the equations (2-30) and (2-31), respectively. Similarly, St is estimated by selecting B as the reference length according to the equation (2-32).

In order to determine the minimum time step size for which reasonable flow pattern is achieved, the same procedure is followed as done for flow about square section. By increasing time step size at initial non-dimensional time step size of 0.001, it is seen that the DVM solution is not stable for Δt^* smaller than 0.02 which is the lower limit of this section. It is seen that smaller time step size introduces too much noise on the solution similar to the case which is conducted for the square section. The spectra of drag coefficient obtained by performing FFT analysis are given in Table 4-4 and the dominant frequency of the oscillation becomes clearer for the simulation with Δt^* greater than 0.04.

Table 4-4. *Comparison of aerodynamic properties of DVM solution of flow over the bridge deck section for different Δt^**

Study	C_{Davg}	C_{Lavg}	St
DMI and SINTEF (1993) Exp	0.54	0.01	0.15
Terrés-Nícoli & Kopp (2009) Exp	-	0.08 – 0.10	0.15
Morgenthal & Mcrobie (2002) DVM	0.42	0.08	0.19
DVM (Δt^*=0.02)	0.36	-0.05	0.17
DVM (Δt^*=0.04)	0.41	-0.07	0.16
DVM (Δt^*=0.06)	0.41	-0.07	0.08
DVM (Δt^*=0.08)	0.46	0.06	0.10
DVM (Δt^*=0.10)	0.46	0.06	0.12
DVM (Δt^*=0.12)	0.48	0.07	0.13
DVM (Δt^*=0.14)	0.50	0.12	0.16
DVM (Δt^*=0.20)	0.56	0.23	0.15

It is noted that negative lift forces are found for DVM solution with Δt^* between 0.02 and 0.06 contrary to several investigations whose results are given in Table 4-4. Moreover, the sign is changed for Δt^* equal and greater than 0.08 although the value of C_{Lavg} does not agree well with experiments. A similar case was experienced by Morgenthal and Mcrobie (2002) in their DVM results given in Table 4-4. In fact, the lift force is developed mostly on the upper and lower faces; therefore, it can be explained by investigating the pressure distributions on those faces.
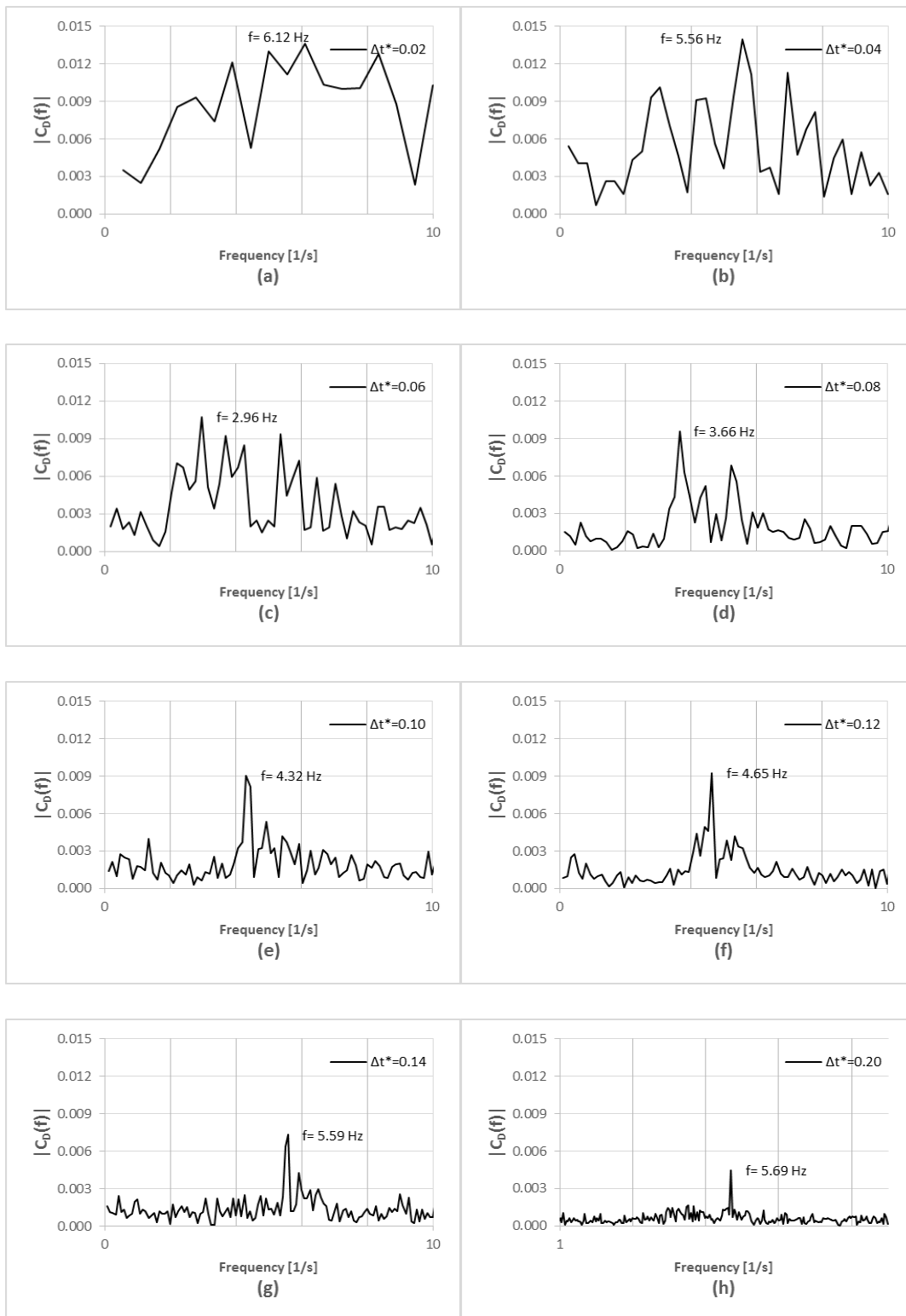
Figure 4-22. Spectra of lift coefficients (C_D) corresponding to Δt^*

The average pressure distribution obtained from DVM simulation with different time step size given in Figure 4-23 and experimental results of two wind tunnel tests conducted by other researchers are given in Figure 4-24 and Figure 4-25. In order to compare the results more precisely, the reference C_P values are given at left bottom of all figures. There are three important features seen on the numerical and experimental pressure distribution. The one of them is that mean pressure over all faces is underestimated for Δt^* smaller than 0.10 and it becomes comparable for Δt^* between 0.10 and 0.14 in terms of its magnitude. Another important aspect is seen on the bottom leading face in such a way that there exist negative and positive wall pressure zones for Δt^* between 0.10 and 0.14 in good agreement with the experiment. In addition, the wall pressure tends to increase for increasing Δt^* with removing the suction on the lower part of it. This may also be the symptom of increase in mean drag coefficient for greater Δt^*. Finally, it is noted that time step size does not have any influence on the incompatibility of present computational and other experimental pressure distributions on the leading edges of top and bottom surface as discussed earlier.

$C_p = -1$ $\Delta t^* = 0.02$

$C_p = -1$ $\Delta t^* = 0.04$

$C_p = -1$ $\Delta t^* = 0.06$

$C_p = -1$ $\Delta t^* = 0.08$

$C_p = -1$ $\Delta t^* = 0.10$

$C_p = -1$ $\Delta t^* = 0.12$

$C_p = -1$ $\Delta t^* = 0.14$

$C_p = -1$ $\Delta t^* = 0.20$
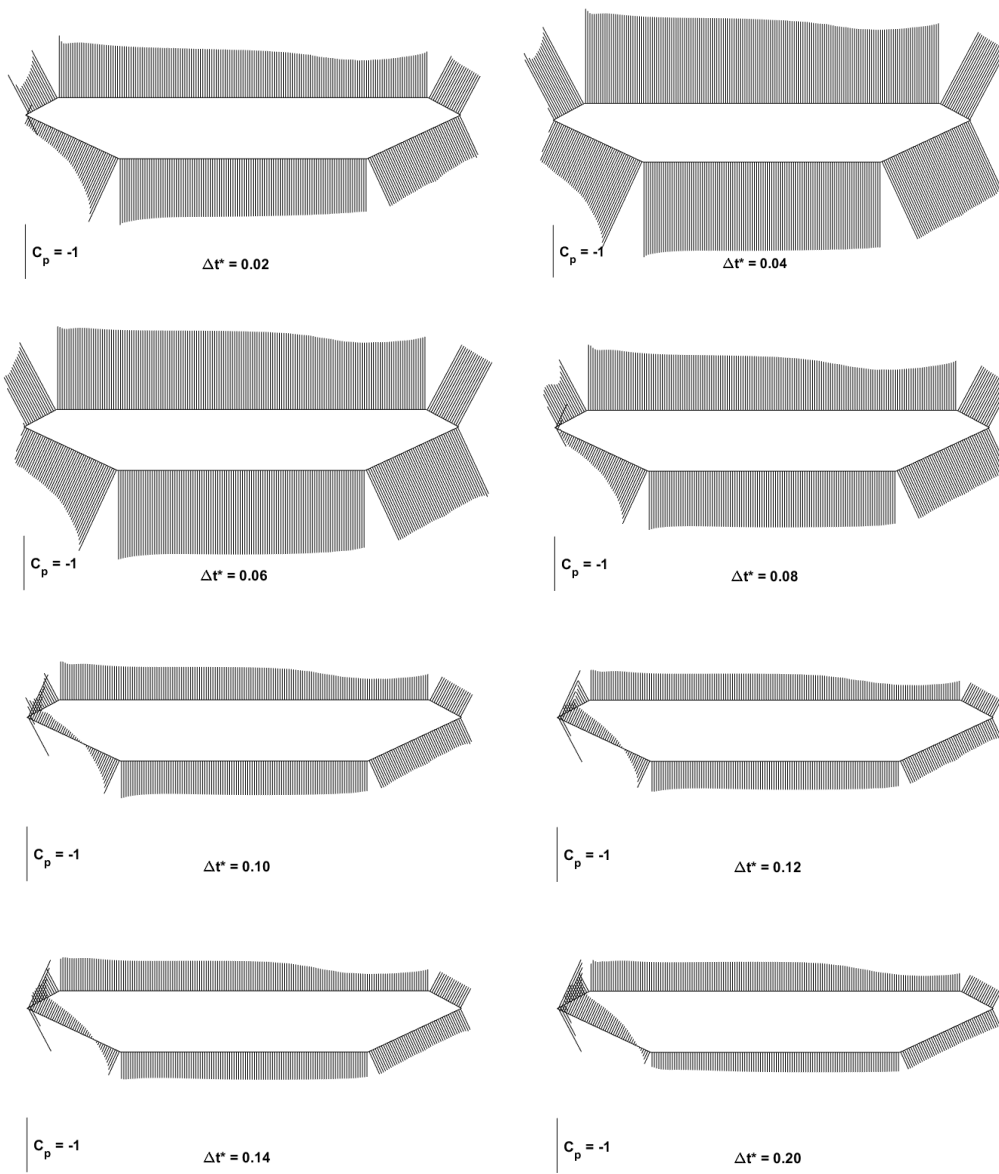
Figure 4-23. Distribution of average pressure coefficient (C_P) for different non-dimensional time step size (Δt^*)
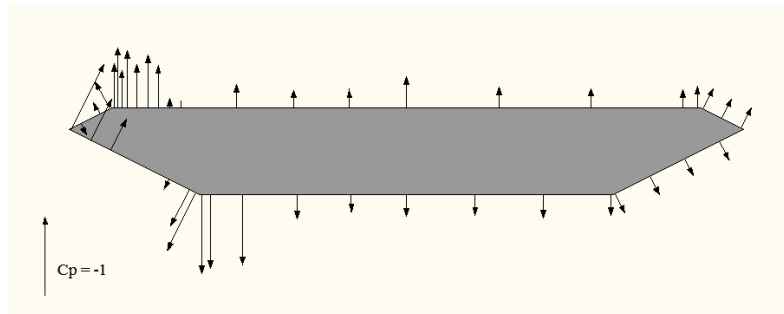
Figure 4-24. Average pressure distribution obtained from wind tunnel experiment with 1:70 scaled section model conducted by Terrés-Nícoli & Kopp *(2009)*
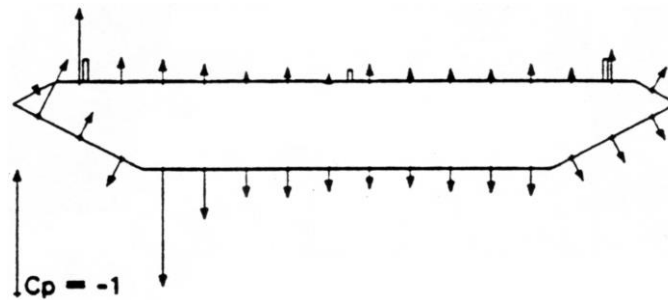
Figure 4-25. Average pressure distribution obtained from wind tunnel experiment with 1:80 scaled section model conducted by DMI and SINTEF *(1993)*

4.2.2. Panel Size

In this section, the effect of panel size on the DVM solution of the bridge deck section is conducted and, in each simulation, equal panel discretization is carried out. The length scaled parameters are not related to each other since panel size is the only control parameter. In the previous section, the most consistent results are obtained for $\Delta t^*=0.14$ as also used in this section. Grid spacing is also selected to be same in the previous section as 0.05D.

DVM model is initiated with number of 50 panels and increased up to 200 at the first stage. It is seen that the results are not stable and reasonable flow pattern is not achieved for panel number (N) is less than 200. It is also noted that DVM solution

69

with N=200 reveals a rapid transition to regular flow pattern compared to N=175. A similar situation is experienced for parametric study of square section, and it is attributed to domination of sheet diffusion over vorticity transfer near the vicinity of the wall leading to instability. Thus, parametric study is conducted for panel numbers between 200 and 1000 in this section.

Table 4-5. *Comparison of aerodynamic properties of DVM solution of flow over the bridge deck section for different panel numbers*

Study	C_{Davg}	C_{Lavg}	St
DMI and SINTEF (1993) Exp	0.54	0.01	0.15
Terrés-Nícoli & Kopp (2009) Exp	-	0.08 – 0.10	0.15
Morgenthal & Mcrobie (2002) DVM	0.42	0.08	0.19
DVM (200 Panels)	0.49	-0.10	0.16
DVM (250 Panels)	0.49	-0.12	0.16
DVM (300 Panels)	0.48	-0.06	0.16
DVM (350 Panels)	0.48	-0.01	0.16
DVM (400 Panels)	0.50	0.12	0.16
DVM (450 Panels)	0.49	0.15	0.16
DVM (500 Panels)	0.49	0.10	0.15
DVM (600 Panels)	0.50	0.14	0.15
DVM (750 Panels)	0.49	0.09	0.15
DVM (1000 Panels)	0.50	0.10	0.15

The mean force coefficients and St obtained from DVM simulations for different panel numbers are given in Table 4-5. It is seen that panel size does not have a considerable effect on the mean drag coefficient and St compared to mean lift coefficient. Although increasing panel numbers affect mean lift coefficient up to N=400, in the following increases in panel numbers it varies between 0.09 – 0.15. The same effect is observed on the mean pressure distribution such that it tends to preserve the shape with negligible changes in magnitude on the top and bottom surface. Therefore, it is

concluded that present DVM solution becomes stable for panel numbers greater than 350 and $\Delta t^*=0.14$.
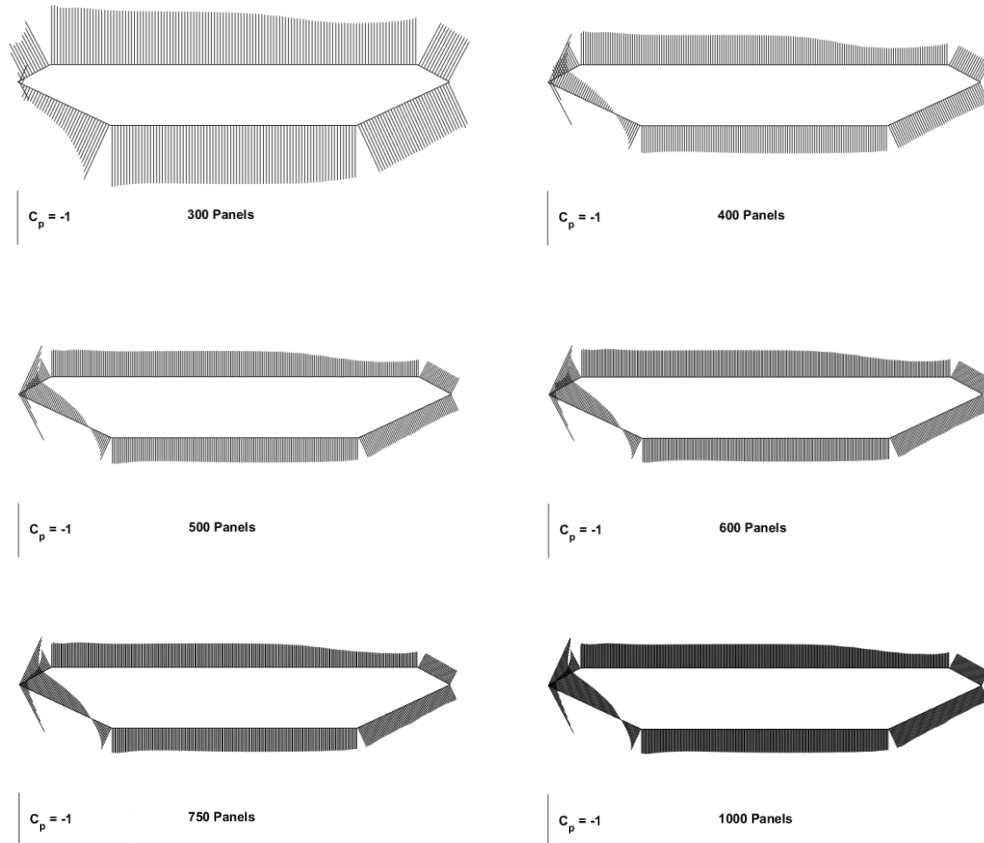

Figure 4-26. Distribution of mean pressure coefficient (C_P) for different panel numbers

4.2.3. Effect of Grid Size

In this section, effect of grid size on DVM solution of flow over the bridge deck section is conducted. In all DVM simulations, domain of the grid system is kept constant by adjusting the number of grids which have equal spacing in both directions.

In the previous sections, effect of panel size and time step size are analyzed for DVM simulations of flow over the bridge deck section. Initially, the effect of time step size is discussed and based on the results obtained from DVM simulations, consistent solutions is obtained for $\Delta t^*=0.14$ compared to other experimental and numerical results. Later, effect of panel size is discussed for DVM simulations with $\Delta t^*=0.14$ and it is seen that panel number greater than 400 does not any notable influence on the solution. Thus, effect of grid size is studied on DVM solution with $\Delta t^*=0.14$ and N=400. DVM solution is also obtained without using grid system and results of grid based and non-grid solution are compared.

Average force coefficients and St obtained from DVM solutions are presented in Table 4-6. It is clearly seen that non-grid DVM solution gives the most favorable results in terms of given aerodynamic quantities compared to the results of other investigations. In the previous sections, relatively good results were obtained in terms of mean drag coefficient and St. On the other hand, it has been seen that effect of control parameters were mostly about pressure distributions and mean lift coefficients. Non-grid DVM solution performs very well on not only mean lift coefficient but also pressure distribution presented in Figure 4-27 (see Figure 4-24 and Figure 4-25 for experimental results).

Table 4-6. *Comparison of aerodynamic properties of DVM solution of flow over the bridge deck section for different grid size*

Study	C_{Davg}	C_{Lavg}	St
DMI and SINTEF (1993) Exp	0.54	0.01	0.15
Terrés-Nícoli & Kopp (2009) Exp	-	0.08 – 0.10	0.15
Morgenthal & Mcrobie (2002) DVM	0.42	0.08	0.19
DVM (non-grid)	0.51	0.03	0.15
DVM (0.0125D)	0.49	0.04	0.15
DVM (0.025D)	0.49	0.07	0.16
DVM (0.05D)	0.50	0.12	0.16
DVM (0.10D)	0.30	0.21	0.01
DVM (0.20D)	0.07	0.33	0.01

Starting with grid size of 0.05D, it is seen that the results of DVM tends to approach non-grid simulation for decreasing grid size. In fact, this is an expected feature since representativeness of grid cell is reduced to finer scales with fewer vortices. Present DVM solution with grid size of 0.0125D gives consistent results with experiments and reveals a negligible loss of accuracy compared to non-grid DVM solution. Considering the fact that decreasing grid spacing costs to increase in total computation time and no considerable change is expected, grid spacing of 0.0125D is determined as lower limit of the present work.

In the wind tunnel tests, there exist the suction peaks on the leading edge of top and bottom surfaces (see Figure 4-24 and Figure 4-25) and a sudden pressure recovery is recorded. Non-grid DVM simulation predicts this feature better than other grid-based solutions. On the other hand, the length of separation bubble on the top and bottom surface tends to decrease for decreasing grid size and approach to the experiments. Instantaneous flow patterns for grid spacing 0.0125D and 0.05D are given in Figure 4-28. It can be seen that for grid size of 0.05D, reattachment of flow takes place away from the midpoint of upper surface and shear layer on the bottom surface seems to

extend beyond the trailing edge. It is attributed to coarse discretization of velocity field which results in poor resolution vortex formation and flow separation developed at fine scale. For the same reason, the results obtained from DVM with grid size greater than 0.05D are inconsistent with the experiments.
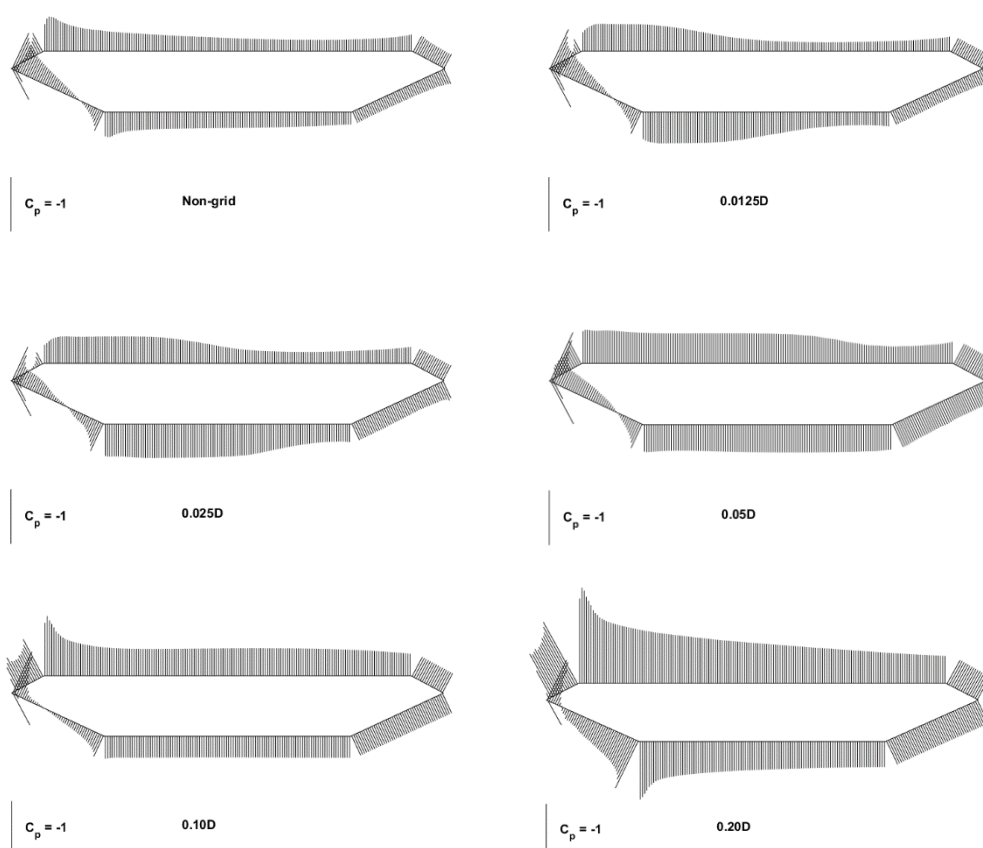

Figure 4-27. Distribution of average pressure coefficient (C_P) for different grid size
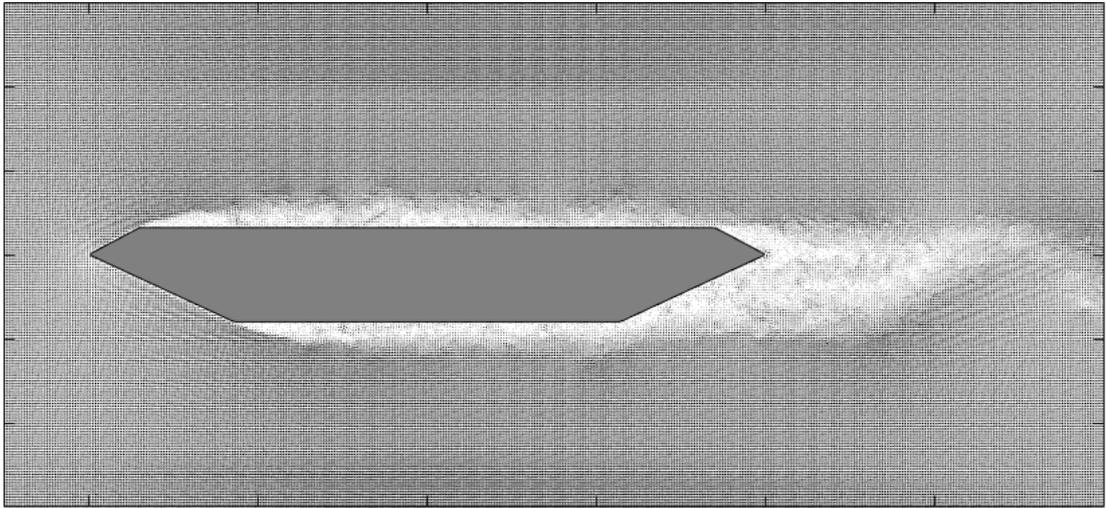
(a)
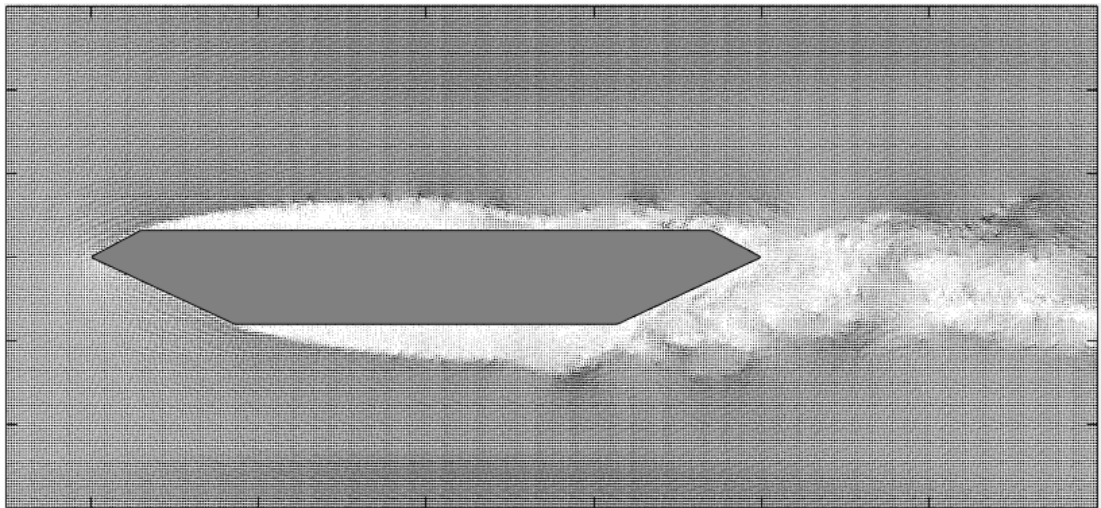
(b)

Figure 4-28. Instantaneous Flow Pattern (a) at t*= 234 for grid spacing 0.0125D (b) at t*= 216 for grid spacing 0.05D
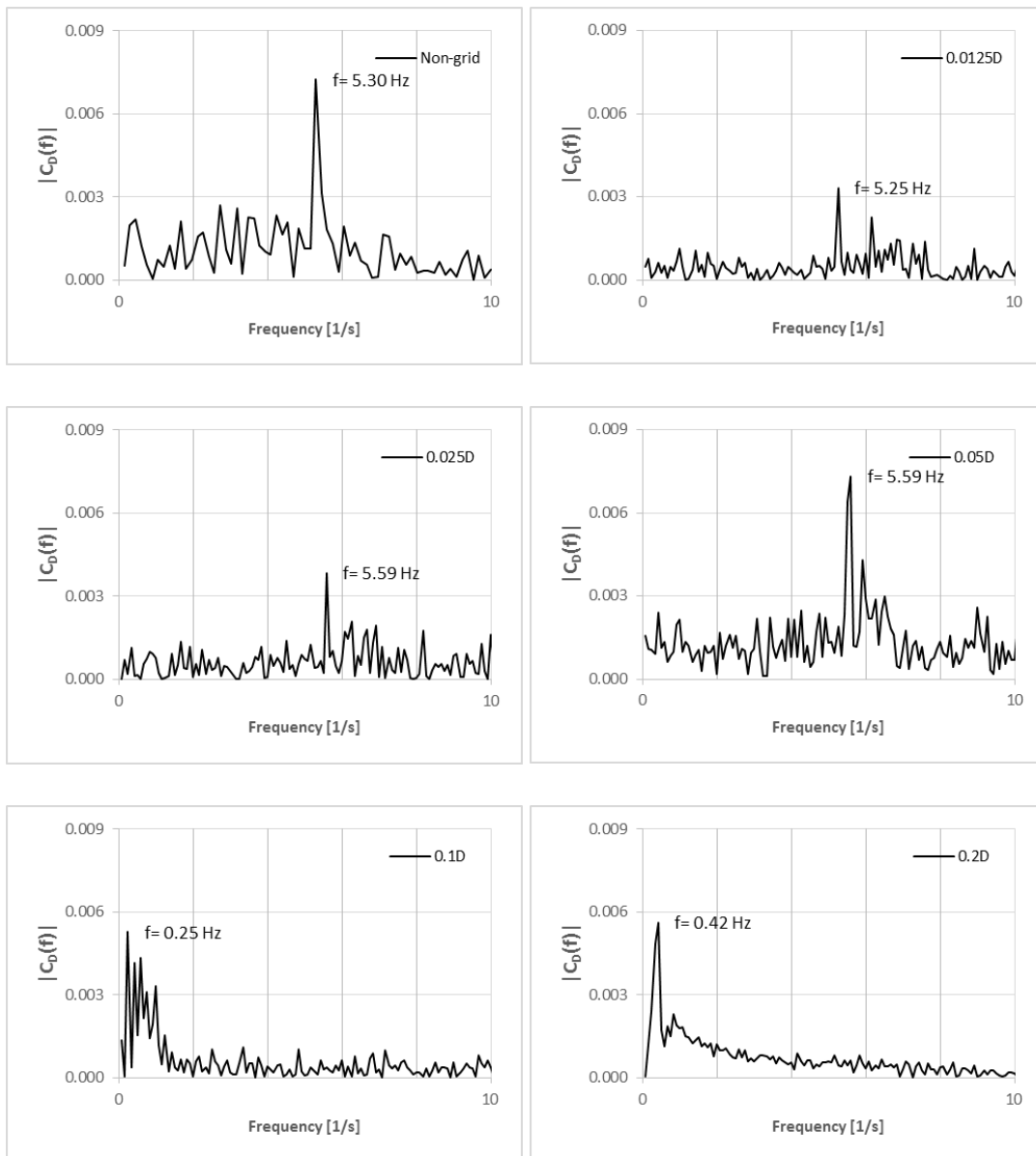
Figure 4-29. Spectra of drag coefficients (C_D) corresponding to grid size

CHAPTER 5

CONCLUSION

5.1. Summary

In this study, aerodynamic analysis of incompressible, viscous flow around rectangular sections and bridge deck section are conducted by using DVM with viscous formulation of Random Walk Technique. Firstly, DVM algorithm developed within the context of this thesis is examined under the validation studies. The results obtained from the DVM simulations with predefined initial parameters are compared with the experimental results. It is seen that the results obtained from present numerical simulations agree reasonably well with experiments in terms of pressure distribution and aerodynamic forces. After satisfying applicability of the algorithm by the validation procedure, flow feature, and aerodynamic quantities are analyzed under cases in which different initial model parameters are used. Conclusion from these parametric studies can be summarized as follows:

- Time step size has a significant influence on the stability and consistency of DVM results. The physical quantities are obtained consistently within a range of non-dimensional time step size. The range is shown to vary between simulations for different body geometry and Re. For smaller time step size, the solution becomes noisy and unreasonable, since the random walk displacements become more significant compared to the convective displacements of the particles. On the other hand, numerical solution loses its ability to capture important fluid actions such as flow separation and formation of vortex structure, and to present development of the vortices near the surfaces. Changing time step size results in disproportionate effect on diffusive

and convective displacements such that diffusion becomes significant for small time steps, on the other hand convection dominates particle displacements for large time step. The possible solution to this problem is using sub-time-steps for diffusion process.

- Sufficient number of panels changes with the body geometry and it is illustrated that while increasing the panel numbers, the rapid transition to reasonable flow pattern and flow quantities are achieved. In addition, increasing number of panels reduces the noise of the solution and gives consistent results. However, after a certain point further increase in panel number does not have any notable effects on aerodynamic force coefficients and wake frequency. In general, present DVM algorithm performs poorly in predicting average pressure distribution for high suction portion of top and bottom faces. One possible solution to this problem is using finer panel size near the corners rather than using same panel size as present study. However, irregular panel size clearly conflicts with satisfactory set of length scaled parameters.

- Although grid system is mainly used for speeding up the convection calculations, in this study its effect on the flow solution is analyzed. It is seen that the most consistent results are obtained for all non-grid numerical simulations. However, loss of accuracy in estimated average force coefficients is negligible for gird-based simulations with small grid size. On the other hand, difference between grid-based and non-grid simulation becomes more significant for the bridge deck section compared to the square section. It is attributed to inability of grid-based simulations to capture small scale flow development around the body surface especially for more complex geometries.

5.2. Recommendation for Future Works

In order to extend the use of present DVM algorithm to different wind engineering problems and to increase its accuracy, recommended future works are listed below:

- Convection calculations are the most time-consuming process in DVM simulations. Grid-based convection schemes are effective in speeding up of the process, but uniform grid size may not suite for flow over complex bodies. Adaptive grid size could be used to increase the accuracy by increasing only the resolution of important regions such as rapidly changing body surface rather than whole domain.

- The calculations could be performed on the parallel computing environment which can reduce total simulation time.

- Diffusion equations could be solved by deterministic methods rather than probabilistic approach applied in present study.

REFERENCES

Batchelor, G. K. (1970). *An introduction to fluid dynamics.* Cambridge University Press.

Bearman, P., & Trueman, D. (1972). An invastigation of the flow around rectangular cylinders. *Aeronautical Quarterly, 23*, 229-237.

Chang, C. (1988). Random vortex method for the Navier-Stokes equations. *Journal of Computational Physics, 76*, 281-300.

Chorin, A. J. (1973). Numerical study of slightly viscous flow. *Journal of Fluid Mechanics, 57*, 785-796.

Christiansen, I. (1973). Numerical simulation of hydrodynamics by the method of point vortices. *Journal of Computational Physics, 13*(3), 363-379.

Deffenbauch, F. D., & Marshall, F. J. (1976). Time development of the flow about an impulsively started cylinder. *AIAA Journal, 14*(7), 908-913.

DMI and SINTEF. (1993). *Wind-tunnel tests, Storeboelt East Bridge, Detailed Design Suspension Bridge Section Model Tests.*

Fogelson, A. L., & Dillon, R. (1993). Optimal smoothing in function-transport particle methods for diffusion equations. *Journal of Computational Physics, 109*, 155-163.

Goodman, J. (1987). Convergence of the random vortex model. In *Communications on Pure and Applied Mathematics, XL* (pp. 189-220). J. Wiley.

Hald, O. H. (1984). *Convergence of a random method with creation of vorticity.* California: Lawrance Berkeley Laboratory, U.C. Berkeley.

Hucho, W. H., & Sovran, G. (1993). Aerodynamics of road vehicles. *Annu. Rev. Fluid Mech., 25*, 485-537.

Jenssen, C. B., & Kvelmsdal, T. (1999). Computational methods for fsi-simulations of slender bridges on high performance computers. *Computational Methods for Fluid-Structure Interaction* (s. 31-40). içinde Tapir.

Karman. (1912). *Uber den echanismus des widerstandes den ein bewegter koerper in einer fluessugkeit erfaehrt.* Göttingen: Nachricht der Koeniglichen Gesellschafet der Wissenschaft.

Kaya, H. (2012). *Aerodynamic analysis of long-span bridge cross-sections using random vortex method.* Middle East Technical University.

Kirchhoff, G. (1869). On the Theory of Free Jets of Fluid. *70*, 289-298.

Larsen, A., & Walther, J. H. (1998). Discrete vortex simulation of flow around five generic bridge deck sections. *Journal of Wind Engineering and Industrial Aerodynamics, 77-78*, 591-602.

Lee, B. (1974). The effect of turbulence on the surface pressure field of a square prsim. *J. Fluid Mech., 69*, 263-282.

Leonard, A. (1980). Vortex methods for flow simulation. *Journal of Computational Physics, 37*(3), 289-335.

Lewis, R. I. (1991). *Vortex Element Methods for Fluid Dynamic Analysis of Engineering Systems.* Cambridge: Cambridge University Press.

Martensen, E. (1959). Calculation of the pressure distribution over profile in cascade in two-dimensional potential flow by means of a Fredholm Integral Equation. *Zweiter Art. Arch. Rat. Anal., 3*(3), 235-270.

Morgenthal, G. (2000). *Fluid-structure interaction in bluff-body aerodynamics and long-span bridge design: Phenomena and methods.* Department of Engineering. Cambrdige: University of Cambridge.

Morgenthal, G., & Mcrobie, F. A. (2002). A comprative study of numerical methods for fluid structure interaction analysis in long-span bridge design. *Wind and Stuructures An International Journal*(5), 101-114.

Naudascher, Y., & Rockwell, D. (1994). *Flow induced vibration - An engineering guide.* Balkema.

Norberg, C. (1993). Flow around rectangular cylinders: Pressure forces and wake frequencies. *Journal of Wind Engineering and Industrial Aerodynamics, 49*, 187-196.

Okajima, A. (1982). Strouhal numbers of rectangular cylinders. *J. Fluid Mech., 123*(379-398).

Porthouse, D. (1983). *Numerical simulation of aerofoil and bluff body flows by vortex dynamics.* University of Newcastle upon Tyne.

Porthouse, D. T., & Lewis, R. I. (1981). Simulation of viscous diffusion for extension of the surface vorticity method to boundary and seperated flows. *J. Mech. Eng. Sci., 23*(3), 157-167.

Reynolds, O. (1883). An experimental investigation of the circumstances which determine whether the motion of water shall be direct or sinuous and of the law of resistance in parallel channels. *Proc. R. Soc. Lond., 35*, 84-89.

Roberts, S. (1985). Accuracy of the random vortex method for a problem with non-smooth inital conditions. *Journal of Computational Physics, 58*, 29-43.

Rosenhead, L. (1931). The formation of vortices from a surface of discontinuity. *Proceedings of the Royal Society of London, 134*(823), 170-192.

Schlichting, H. (1979). *Boundary-Layer Theory.* McGraw-Hill.

Shukla, R. K., & Eldredge, J. D. (2007). An inviscid model for vortex shedding from a deforming body. *Theoretical and Computational Fluid Dynamics, 21*(5), 343-368.

Smith, P., & Stansby, P. (1988). Impulsively started flow around a circular cylinder by the vortex method. *Journal of Fluid Mechanics, 194*, 45-77.

Spalart, P. (1988). Vortex methods for seperated flows. *NASA TM 100068.*

Spalart, P., & Leonard, A. (1981). Computation of separated flows by a vortex-tracing algorithm. *AIAA 14th Fluid and Plasma Dynamics Confrence.* California.

Stansby, P., & Dixon, A. (1983). Simulation of flows around cylinders by a Lagrangian vortex scheme. *Applied Ocean Research, 5*(3), 167-178.

Strouhal, V. (1878). On a particular way of tone generation. *Annalen der Physik und Chemie, 5*, 216-251.

Tamura, T., & Miyagi, T. (1999). The effect of turbulence on aerodynamic forces on a square cylinder with various corner shapes. *Journal of Wind Engineering and Industrial Aerodynamics, 83*, 135-145.

Taylor, I. J. (1999). *Study of bluff body flow fields and aeroelastic stability using a discrete vortex method.* Department of Aerospace Engineering. Glasgow: University of Glasgow.

Taylor, I., & Vezza, M. (1999). Prediction of unsteady flow around square and rectangular section cylinders using a discrete vortex method. *Journal of Wind Engineering and Industrial Aerodynamics, 82*, 247-269.

Terrés-Nícoli , J. M., & Gregory, A. K. (2009). Mechanisms of the Vertical Vortex Induced Vibration of the Storebælt Bridge. *11th Americas Confrence on Wind Engineering.* San Juan.

Vickery, B. J. (1966). Fluctuating lift and drag on a long cylinder of square cross-section in a smooth and in a turbulent stream. *J. Fluid Mech., 25*, 481-494.

APPENDICES

A. Preparation of Input Data

Before running the simulations, the files including the surface data and input parameters are prepared and moved to the execution folder. The parameters and the variables in the input file are presented in *Table A.1*.

Table A.1. *Model parameters and variables*

Parameter / Variable	Description in input file	Unit
Name of body file	BODYFILE	-
Total number of time step	TIMESTEP	-
Time step size	TIMESTEPSIZE	s
Panel number	PANELNUMBER	-
X-component of free stream velocity	UINF	m/s
Y-component of free stream velocity	VINF	m/s
Kinematic viscosity	VISC	m^2/s
Fluid density	RHO	kg/m^3
Core radius	RCORE	m
Merging flag (0/1)	MERGE	-
Merging limit distance	DMERGE	m
Shedding distance from the surface	EPSILON	m
X coordinate of grid generation base point	XGRID0	m
Y coordinate of grid generation base point	YGRID0	m
Grid spacing	GRIDDS	m
Number of grid points in x-direction	XGRIDNO	
Number of grid points in y-direction	YGRIDNO	

First step of the model simulation process is preparation of body file. Body file consists of the coordinates of data points which are used to define panels' length, their orientation and pivotal points in the main program. Together with name of the body file, other model inputs and variables are specified in the input file.

B. Post-processing

After the model runs are successfully completed, the results obtained from each time step are used in post-processing tools which are developed in MATLAB programming language. There are 4 type of output files generated by the simulations. Output files starting with "CP" which are generated at each time step include pressure coefficient of each panel. For comparison analysis, pressure coefficients at each panel for total time is constructed by reading all pressure output files. The position and strength of vortices are stored in the files starting with "Output" which are generated at each time step. These files are used to visualize flow field for a time step. Velocity field is determined by applying Biot-Savart law for non-grid DVM simulations corresponding to the post-defined grids. On the other hand, the velocity components in the grid points which are pre-defined and used for convection calculations are stored in the files starting with "Vout". Finally, force coefficients are stored in a single file named as "Pressure" and updated at each time iteration by appending the current values in a new line. However, the values are estimated for unit characteristic length. Therefore, the actual values are re-estimated via post-processing tools by dividing the post-defined characteristic lengths.